Separable representation of multichannel nucleon-nucleus optical potentials

L. Hlophe[1,*] and Ch. Elster[2,†]

[1]*National Superconducting Cyclotron Laboratory and Department of Physics and Astronomy, Michigan State University, East Lansing, Michigan 48824, USA*

[2]*Institute of Nuclear and Particle Physics, and Department of Physics and Astronomy, Ohio University, Athens, Ohio 45701, USA*

(Received 18 November 2016; revised manuscript received 22 February 2017; published 22 May 2017)

Background: One important ingredient for many applications of nuclear physics to astrophysics, nuclear energy, and stockpile stewardship is cross sections for reactions of neutrons with rare isotopes. Since direct measurements are often not feasible, indirect methods, e.g., (d,p) reactions, should be used. Those (d,p) reactions may be viewed as three-body reactions and described with Faddeev techniques.

Purpose: Faddeev equations in momentum space have a long tradition of utilizing separable interactions in order to arrive at sets of coupled integral equations in one variable. Optical potentials representing the effective interactions in the neutron (proton) nucleus subsystem are usually non-Hermitian as well as energy dependent. Including excitations of the nucleus in the calculation requires a multichannel optical potential. The purpose of this paper is to introduce a separable, energy-dependent multichannel representation of complex, energy-dependent optical potentials that contain excitations of the nucleus and that fulfill reciprocity exactly.

Methods: Momentum space Lippmann-Schwinger integral equations are solved with standard techniques to obtain the form factors for the separable representation.

Results: Starting from energy-dependent multichannel optical potentials for neutron and proton scattering from ^{12}C, separable representations based on a generalization of the Ernst-Shakin-Thaler (EST) scheme are constructed which fulfill reciprocity exactly. Applications to $n + {}^{12}$C and $p + {}^{12}$C scattering are investigated for energies from 0 to 50 MeV.

Conclusions: We find that the energy-dependent separable representation of complex, energy-dependent phenomenological multichannel optical potentials describes scattering data with the same quality as the original potential.

DOI: 10.1103/PhysRevC.95.054617

I. INTRODUCTION

Nuclear reactions are an important probe to learn about the structure of unstable nuclei. Due to the short lifetimes involved, direct measurements are usually not possible. Therefore, indirect measurements using (d,p) reactions have been proposed (see, e.g., Refs. [1–3]). Deuteron-induced reactions are particularly attractive from an experimental perspective, since deuterated targets are readily available. From a theoretical perspective, they are equally attractive because the scattering problem can be reduced to an effective three-body problem [4]. Traditionally deuteron-induced single-neutron transfer (d,p) reactions have been used to study the shell structure in stable nuclei. Nowadays, experimental techniques are available to apply the same approaches to exotic beams (see, e.g., Ref. [5]). Deuteron-induced (d,p) or (d,n) reactions in inverse kinematics are also useful to extract neutron or proton capture rates on unstable nuclei of astrophysical relevance [6]. Given the many ongoing experimental programs worldwide using these reactions, a reliable reaction theory for (d,p) reactions is critical.

One of the most challenging aspects of solving the three-body problem for nuclear reactions is the repulsive Coulomb interaction. While for very light nuclei, exact calculations of (d,p) reactions based on momentum-space Faddeev equations in the Alt-Grassberger-Sandhas (AGS) [7] formulation can be carried out [8] by using a screening and renormalization procedure [9,10], this technique leads to increasing technical difficulties when moving to computing (d,p) reactions with heavier nuclei [11]. Therefore, a new formulation of the Faddeev-AGS equations, which does not rely on a screening procedure, was presented in Ref. [12]. Here the Faddeev-AGS equations are cast in a momentum-space Coulomb-distorted partial-wave representation instead of the plane-wave basis. Thus all operators, specifically the interactions in the two-body subsystems, must be evaluated in the Coulomb basis, which is a nontrivial task. The formulation of Ref. [12] requires the interactions in the subsystems to be of separable form. The same reference suggests an extension of the Faddeev-AGS equations to take excitations of the nucleus into account. Faddeev-AGS calculations taking into account rotational excitations were carried out for (d,p) reactions with ^{10}Be and ^{24}Mg in Refs. [13,14], showing that the inclusion of excited states in those nuclei could improve the description of experimental data.

Taking into account excitations in nuclear reaction calculations has a long-standing tradition leading to formulating the scattering equations as a coupled-channel problem (see, e.g., Refs. [15–17]), and a large body of work in nuclear reactions is based on solving coordinate space coupled-channel differential equations. To include excitations of the nucleus in the formulation of Ref. [12], separable representations of the effective

*hlophe@nscl.msu.edu
†elster@ohio.edu

neutron and proton interactions with the nucleus which include those excitations need to be constructed in momentum space. We follow here work already carried out for single-channel optical potentials that are complex [18] as well as energy dependent [19]. These separable representations have roots in the work by Ernst, Shakin, and Thaler [20] (EST), who derived a scheme for constructing separable representations using scattering wave functions at given energies as basis for their expansion. In momentum space, the scattering wave functions are related to half-shell t matrices. Thus, the EST choice guarantees that, at those fixed energies, the separable expansion is not only on-shell but also half-shell exact. The generalization to complex, energy-dependent optical potentials of Refs. [18,19] fulfills the same conditions and in addition guarantees that reciprocity is fulfilled.

Using scattering wave functions as basis for deriving separable representations is not the only possible choice. Following the work of Refs. [21,22], Sturmian basis functions have recently been used to define a separable multichannel potential for describing low-energy neutron scattering from ^{12}C and successfully capturing the low-lying resonances [23,24].

The goal of this work is to generalize the formulation of Ref. [19] so that excitations of the nucleus can be taken into account in a multichannel framework. Although an extension of the EST scheme to multichannel potentials was already carried out in Ref. [25], that work was limited to Hermitian potentials. In this paper, we want to obtain a separable representation of complex, energy-dependent multichannel optical potentials. First, we derive the formulation for multichannel neutron-nucleus optical potentials in Sec. II and apply the formulation to neutron elastic and inelastic scattering off ^{12}C. In Sec. III, we extend this formulation to charged particle scattering and show as application the elastic and inelastic scattering of protons from ^{12}C. Our findings are summarized in Sec. IV. The paper is accompanied by three appendixes explaining analytic and numerical details.

II. ENERGY-DEPENDENT MULTICHANNEL NEUTRON-NUCLEUS OPTICAL POTENTIALS

A. Formal considerations

1. Coupled-channel formalism

For setting up the multichannel problem, let us consider a nucleus characterized by the spin parity I^π. The nuclear wave function is represented by $|\Phi_{IM_I}\rangle$, where M_I is the projection of I along the z axis. A neutron interacting with the nucleus through a potential U has an angular momentum $j_p = l \pm s$, with l being the relative orbital angular momentum and $s = 1/2$ its spin. The total, conserved angular momentum $\mathbf{J}$ of the system takes values $|I - j_p| \leqslant J \equiv |\mathbf{J}| \leqslant I + j_p$, and its projection along the z axis is given by M. The states of conserved angular momentum are thus given by [16]

$$|(Ilsj_p)JM\rangle = \sum_{M_I m_{j_p}} C\left(Ij_pJ,M_Im_{j_p}M\right)\left|\mathcal{Y}_{ls}^{j_pm_{j_p}}\right\rangle\left|\Phi_{IM_I}\right\rangle, \quad (1)$$

where

$$\left|\mathcal{Y}_{ls}^{j_pm_{j_p}}\right\rangle = \sum_{m_lm_s} C\left(lsj_p,m_lm_sm_{j_p}\right)\left|Y_{lm_l}\right\rangle|sm_s\rangle. \quad (2)$$

The functions Y_{lm_l} are the spherical harmonics, χ_{sm_s} are the corresponding spinors, and $C(lsj_p,m_lm_sm_{j_p})$ are Clebsch-Gordon (CG) coefficients. The quantities I, l, and j_p collectively characterize a particular configuration of the system but are not individually conserved. These configurations make up the angular momentum channels and will be denoted using the Greek letters α, β, γ, etc. Since the potential U couples different angular momentum channels, we need to employ a coupled-channel formulation to describe a scattering process. The multichannel wave function $|\Psi_{\alpha_0}^{J\pi(+)}\rangle$ is characterized by the total angular momentum J, the parity π, as well as the incident angular momentum channel α_0, and obeys a coupled set of Lippmann-Schwinger (LS) equations,

$$\left|\Psi_{\alpha\alpha_0}^{J(+)}\right\rangle = |lk_0\rangle\,\delta_{\alpha\alpha_0} + G_{0\alpha}(E)\sum_{\alpha'} U_{\alpha\alpha'}^J\left|\Psi_{\alpha'\alpha_0}^{J(+)}\right\rangle. \quad (3)$$

Here $|\Psi_{\alpha\alpha_0}^{J(+)}\rangle$ represents a projection of the wave function $|\Psi_{\alpha_0}^{J\pi(+)}\rangle$ onto the α channel. The free propagator in a given channel α has the form $G_{0\alpha}(E) = (E - \varepsilon_\alpha - H_0 + i\epsilon)^{-1}$ with $E = k_0^2/2\mu$ being the nonrelativistic kinetic energy in the incident channel and μ the reduced mass. Here, ε_α designates the nuclear excitation energy in channel α. Using the states of Eq. (3) in the operator LS equation, $T(E) = U + UG_0(E)T(E)$, one obtains a set of coupled t matrix equations:

$$T_{\alpha\alpha_0}^J(E) = U_{\alpha\alpha_0}^J + \sum_{\alpha'} U_{\alpha\alpha'}^J G_{0\alpha'}(E) T_{\alpha'\alpha_0}^J(E). \quad (4)$$

Here $U_{\alpha\alpha_0}^J \equiv \langle\alpha JM|U|\alpha_0JM\rangle$ and $T_{\alpha\alpha_0}^J(E) \equiv \langle\alpha JM|T(E)|\alpha_0JM\rangle$ are elements of the multichannel potential and t matrix respectively. The explicit LS equation for the half-shell t matrix in momentum space takes the form

$$T_{\alpha\alpha_0}^J(k',k;E) = U_{\alpha\alpha_0}^J(k',k) + \sum_{\alpha'}\int_0^\infty dpp^2\, U_{\alpha\alpha'}^J(k,p) \times G_{0\alpha'}(E,p)T_{\alpha'\alpha_0}^J(p,k;E), \quad (5)$$

where the propagator is given by $G_{0\alpha}(E,p) = (E_\alpha - p^2/2\mu_\alpha + i\epsilon)^{-1}$. Here $E_\alpha \equiv E - \varepsilon_\alpha$ is the center of mass (c.m.) energy and μ_α is the reduced mass in channel α. Further details on the scattering of neutrons from deformed nuclei are given in Appendix B.

2. Separable representation of complex, energy-dependent multichannel potentials

For single-channel separable representations, the work of Ref. [18] already showed that the EST scheme presented in Ref. [20] leads to the violation of reciprocity when applied to complex potentials, which can be resolved if both incoming and outgoing scattering states are used in the separable expansion. However, the separable potentials from Ref. [18] still do not completely fulfill reciprocity for energy-dependent potentials. A further generalization of the EST scheme for potentials that are both complex and energy dependent had

to be developed [19], which involves introducing an energy-dependent separable potential

$$u(E) = \sum_{ij} U(E_i)|\psi_i^{(+)}\rangle \lambda_{ij}(E) \langle\psi_j^{(-)}|U(E_j). \tag{6}$$

Here $|\psi_i^{(+)}\rangle$ is an outgoing single-channel scattering wave function corresponding to U at the energy E_i, and $|\psi_i^{(-)}\rangle$ is an incoming single-channel scattering wave function corresponding to U^* at the energy E_i. The energies E_i are referred to as the EST support points. The total number of EST support points defines the rank of the separable potential and thus is the upper limit of the rank indices i and j. Equation (6) shows that the energy dependence is introduced into the coupling matrix elements $\lambda_{ij}(E)$, which obey the constraint

$$\begin{aligned}\mathcal{U}^e_{mn}(E) &= \langle\psi_m^{(-)}|u(E)|\psi_n^{(+)}\rangle \\ &= \sum_{ij}\langle\psi_m^{(-)}|U(E_i)|\psi_i^{+}\rangle \lambda_{ij}(E)\langle\psi_j^{(-)}|U(E_j)|\psi_n^{+}\rangle,\end{aligned} \tag{7}$$

where the matrix elements between in- and outgoing scattering states at energies E_m and E_n are given as

$$\mathcal{U}^e_{mn}(E) \equiv \langle\psi_m^{(-)}|U(E)|\psi_n^{(+)}\rangle. \tag{8}$$

Defining the matrix elements $\mathcal{U}_{mn}$

$$\mathcal{U}_{mn} \equiv \mathcal{U}^e(E_m) = \langle\psi_m^{(-)}|U(E_m)|\psi_n^{(+)}\rangle \tag{9}$$

leads to a more compact form for Eq. (7),

$$\begin{aligned}\mathcal{U}^e_{mn}(E) &= \sum_{ij} \mathcal{U}^t_{mi}\ \lambda_{ij}(E)\, \mathcal{U}_{jn}, \\ &= [\mathcal{U}^t \cdot \lambda(E) \cdot \mathcal{U}]_{mn},\end{aligned} \tag{10}$$

where $\mathcal{U}^t$ represents the transpose of $\mathcal{U}$. This constraint ensures that the eigenstates of U and u coincide at the EST support points. The coupling matrix is symmetric so that $\lambda_{ij}(E) = \lambda_{ji}(E)$, a condition necessary for the fulfillment of reciprocity. Since u is explicitly energy dependent, we coin this representation as energy-dependent EST (eEST) scheme. For single-channel, energy-dependent optical potentials, the on-shell t matrix elements obtained with the eEST scheme and its energy-independent approximation (EST) agree quite well [19].

To generalize the eEST scheme to multichannel potentials, we proceed analogously to Ref. [25] and replace the single-channel scattering wave functions $\psi_i^{(+)}$ and $\psi_j^{(-)}$ with their multichannel counterparts $\Psi^{J\pi(+)}_{\rho,i}$ and $\Psi^{J\pi(-)}_{\sigma,j}$. The indices J and π will be omitted hereafter since the potential U preserves the total angular momentum and parity. The multichannel separable potential is thus given as

$$u(E) = \sum_{\rho\sigma}\sum_{ij} U(E_i)|\Psi^{(+)}_{\rho,i}\rangle\ \lambda^{\rho\sigma}_{ij}(E)\ \langle\Psi^{(-)}_{\sigma,j}|U(E_j). \tag{11}$$

The indices i and j stand for the EST support points as was the case in Eq. (6), while ρ and σ characterize the coupling to different channels. The separable potential of Eq. (11) is defined for a specific conserved total angular momentum and parity J^π. The sum over the channel indices thus includes all angular momentum channels that correspond to a particular J^π. For example, let us consider a system of a neutron and a nucleus with a 0^+ ground state and a 2^+ excited state. For $J^\pi = 1/2^+$, there are 3 coupled channels so that the upper limit for ρ and σ is 3. When evaluating cross sections, many values of J contribute. In this work, the maximum value for J is 13/2, which corresponds to 12 angular momentum channels. The total number of channels required to evaluate cross sections is 76.

Using the definition of the multichannel half-shell t matrix [26],

$$\begin{aligned}T(E_i)\big|\rho\ k_i^\rho\big\rangle &= U(E_i)|\Psi^{(+)}_{\rho,i}\rangle, \\ \big\langle\sigma\ k_j^\sigma\big|T(E_i) &= \langle\Psi^{(-)}_{\sigma,j}|U(E_j),\end{aligned} \tag{12}$$

Eq. (11) can be recast as

$$u(E) = \sum_{\rho\sigma}\sum_{ij} T(E_i)\big|\rho k_i^\rho\big\rangle\ \lambda^{\rho\sigma}_{ij}(E)\ \big\langle k_j^\sigma\ \sigma\big|T(E_j). \tag{13}$$

To determine the constraint on $u(E)$, we first generalize the matrices $\mathcal{U}^e(E)$ and $\mathcal{U}$ defined by Eqs. (8) and (9) to multichannel potentials. This is accomplished by replacing the single-channel scattering states by the multichannel wave functions in the initial and final states, so that

$$\mathcal{U}^{e,\alpha\beta}_{mn}(E) \equiv \langle\Psi^{(-)}_{\alpha,m}|U(E)|\ \Psi^{(+)}_{\beta,n}\rangle \tag{14}$$

and

$$\mathcal{U}^{\alpha\beta}_{mn} \equiv \mathcal{U}^{e,\alpha\beta}_{mn}(E_m) = \langle\Psi^{(-)}_{\alpha,m}|U(E_m)|\Psi^{(+)}_{\beta,n}\rangle. \tag{15}$$

Here Eq. (15) shows that the matrix $\mathcal{U}$ depends only on the support energies E_m and E_n. On other hand, we see from Eq. (14) that $\mathcal{U}^e(E)$ depends on the projectile energy E as well as the support energies. The constraint on the separable potential is obtained by substituting the multichannel matrices $\mathcal{U}^e$ and $\mathcal{U}$ into Eq. (10), leading to

$$\begin{aligned}\mathcal{U}^{e,\alpha\beta}_{mn}(E) &= \sum_{\rho\sigma}\sum_{ij}(\mathcal{U}^t)^{\alpha\rho}_{mi}\ \lambda^{\rho\sigma}_{ij}(E)\, \mathcal{U}^{\sigma\beta}_{jn}, \\ &= [\mathcal{U}^t \cdot \lambda(E) \cdot \mathcal{U}]^{\alpha\beta}_{mn}.\end{aligned} \tag{16}$$

To evaluate the separable multichannel t matrix, Eqs. (13) to (16) are inserted into Eq. (4) to give

$$\begin{aligned}t(E) &= \sum_{\rho\sigma}\sum_{ij} U(E_i)|\Psi^{(+)}_{\rho,i}\rangle\ \tau^{\rho\sigma}_{ij}(E)\ \langle\Psi^{(-)}_{\sigma,j}|U(E_j), \\ &= \sum_{\rho\sigma}\sum_{ij} T(E_i)\big|\rho k_i^\rho\big\rangle\ \tau^{\rho\sigma}_{ij}(E)\ \big\langle k_j^\sigma\ \sigma\big|T(E_j).\end{aligned} \tag{17}$$

The coupling matrix elements $\tau^{\rho\sigma}_{ij}(E)$ are implicitly defined by

$$R(E) \cdot \tau(E) = \mathcal{M}(E), \tag{18}$$

where

$$\begin{aligned}R^{\rho\sigma}_{ij}(E) = \big\langle k_i^\rho\big|T_{\rho\sigma}(E_i) &+ \sum_\beta T_{\rho\beta}(E_i)G_\beta(E_j)T_{\beta\sigma}(E_j)\big|k_j^\sigma\big\rangle \\ &- \sum_{\beta\beta'}\sum_n \mathcal{M}^{\rho\beta}_{in}\big\langle k_n^\beta\big|T_{\beta\beta'}(E_n)G_{\beta'}(E)T_{\beta'\sigma}(E_j)\big|k_j^\sigma\big\rangle\end{aligned} \tag{19}$$

and

$$\mathcal{M}_{ij}^{\rho\sigma}(E) = [\mathcal{U}^e(E)\cdot\mathcal{U}^{-1}]_{ij}^{\rho\sigma}. \quad (20)$$

The expression for the matrix $R_{ij}^{\rho\sigma}(E)$ is analogous to the one obtained in Ref. [19] for the single-channel case except for the extra channel indices.

The eEST scheme simplifies considerably for energy-independent potentials. From Eqs. (14) we see that the dependence of the separable potential u on the scattering energy E arises from the energy dependence of U. Consequently, the separable potential is independent of the energy E if U is energy independent. To derive the multichannel EST separable representation for energy-independent potentials, we set

$$U(E) = U(E_i) = U(E_j) = U(E_m) = U \quad (21)$$

in Eq. (15). This leads to

$$\mathcal{U}_{mn}^{\alpha\beta} \equiv \mathcal{U}_{mn}^{e,\alpha\beta} = \langle\Psi_{\alpha,m}^{(-)}|U|\Psi_{\beta,n}^{J(+)}\rangle, \quad (22)$$

which implies that the matrices $\mathcal{U}$ and $\mathcal{U}^e$ are identical. As a consequence, the matrix $\mathcal{M}$ in Eq. (20) reduces to an identity matrix. The energy-independent separable potential takes the form

$$u(E) = \sum_{\rho\sigma}\sum_{ij} T(E_i)\big|\rho k_i^\rho\big\rangle\,\lambda_{ij}^{\rho\sigma}(E)\,\big\langle k_j^\sigma\,\sigma\big|T(E_j), \quad (23)$$

with the constraint

$$\delta_{\alpha\beta}\delta_{mn} = \sum_{i\rho}(\mathcal{U}^t)_{mi}^{\alpha\rho}\,\lambda_{in}^{\rho\beta}. \quad (24)$$

The corresponding separable t matrix is given by Eq. (17). The coupling matrix $\tau(E)$ is obtained by replacing the matrix $\mathcal{M}$ in Eqs. (18) and (19) with the identity matrix so that

$$R(E)\cdot\tau(E) = \mathbf{1}. \quad (25)$$

The matrix elements $R_{ij}^{\rho\sigma}(E)$ are given as

$$R_{ij}^{\rho\sigma}(E) = \big\langle k_i^\rho\big|T_{\rho\sigma}(E_i) + \sum_\beta T_{\rho\beta}(E_i)G_\beta(E_j)T_{\beta\sigma}(E_j)\big|k_j^\sigma\big\rangle - \sum_\beta\sum_n \big\langle k_n^\rho\big|T_{\rho\beta}(E_n)G_\beta(E)T_{\beta\sigma}(E_j)\big|k_j^\sigma\big\rangle. \quad (26)$$

Since the separable potential does not depend on the scattering energy E, we refer to this scheme as the energy-independent EST separable representation. Although it is derived for energy-independent potentials, it can be applied to energy-dependent ones as well since only the multichannel half-shell t matrices are required as input. The consequences of applying the energy-independent EST separable representation scheme to energy-dependent potentials were investigated in Ref. [19] for single-channel optical potentials. It was determined that the off-shell t matrix was not symmetric and thus violated the reciprocity theorem. Here a similar study will be carried out for multichannel neutron optical potentials.

3. *Simple illustration for implementing the multichannel eEST scheme*

The eEST separable representation scheme in Sec. II B for the potential and the t matrix is derived for arbitrary rank as well as an arbitrary number of coupled channels, and thus looks quite complicated. To demonstrate a simple implementation, we want to consider a case where there are only two coupled angular momentum channels, as would occur in the scattering of neutrons and protons in the triplet channel. To further simplify, we restrict the rank of the separable potential to one EST support point E_1. This means that the channel indices have the domain $1 \leqslant \alpha, \beta, \rho, \sigma \leqslant 2$, while all other indices i, j, m, and n are equal to one. The goal is to use the multichannel eEST scheme to construct a multichannel separable potential $u(E)$ starting from an otherwise nonseparable, complex, and energy-dependent multichannel potential $U(E)$. The separable potential is then used to obtain the separable t matrix by evaluating Eqs. (17) to (20). The momentum space expressions for the separable t matrix are given by Eqs. (B4) and (B5). In our example, the input consists of the four half-shell t matrices $T_{11}(E_1)$, $T_{21}(E_1)$, $T_{12}(E_1)$, and $T_{22}(E_1)$, which are obtained by solving the coupled-channel LS equation, Eq. (5), with the starting potential $U(E)$. This allows the evaluation of the matrix elements $R_{11}(E)$, $R_{12}(E)$, $R_{21}(E)$, and $R_{22}(E)$ using Eq. (B4). The coupling matrix elements τ_{11}, τ_{12}, τ_{21}, and τ_{22} can then be computed from Eq. (B1). Finally, we employ Eq. (B5) to obtain the multichannel separable t matrix

$$\begin{aligned} t_{\alpha\beta}(k',k;E) &= T_{\alpha1}\big(k',k_1^{(1)};E_1\big)\,\tau_{11}(E)\,T_{1\beta}(E_1) \\ &\quad + T_{\alpha1}\big(k',k_1^{(1)};E_1\big)\,\tau_{12}\big(k',k_1^{(2)};E\big)\,T_{2\beta}\big(k',k_1^{(1)};E_1\big) \\ &\quad + T_{\alpha2}\big(k',k_1^{(2)};E_1\big)\,\tau_{21}(E)\,T_{1\beta}\big(k',k_1^{(1)};E_1\big) \\ &\quad + T_{\alpha2}\big(k',k_1^{(2)};E_1\big)\,\tau_{22}(k',k;E)\,T_{2\beta}\big(k',k_1^{(2)};E_1\big). \end{aligned} \quad (27)$$

Here $k_1^{(1)}$ and $k_1^{(2)}$ are the on-shell momenta corresponding to E_1 in channels 1 and 2. The matrix elements $t_{11}(k',k;E)$, $t_{21}(k',k;E) = t_{12}(k,k';E)$, and $t_{22}(k',k;E)$ are obtained from Eq. (27). Applying the eEST scheme to realistic multichannel nucleon-nucleus optical potentials involves many more angular momentum channels and EST support points. Nonetheless, the procedure is similar to the simple example considered here.

B. Application to the elastic and inelastic scattering of neutrons from ^{12}C

In this section, we demonstrate that the eEST scheme introduced in Sec. II A 2 can be successfully employed to create high-quality separable representations of multichannel neutron optical potentials. As an example, we consider the scattering of neutrons from the nucleus ^{12}C. The ^{12}C nucleus possesses selected excited states, with the first and second levels having $I^\pi = 2^+$ and $I^\pi = 4^+$ and being located at 4.43 and 14.08 MeV above the 0^+ ground state. The collective rotational model [27] is assumed to describe the coupling between the ground state and these excited states. The deformed optical model potential (DOMP) by Olsson [28] is a coupled-channel optical potential and is adopted to describe the $n + {}^{12}$C interaction. It is based on the rigid rotor model and fits its parameters to elastic and inelastic neutron scattering data between 16 and 22 MeV laboratory kinetic energy. Since different angular momentum channels are coupled, it

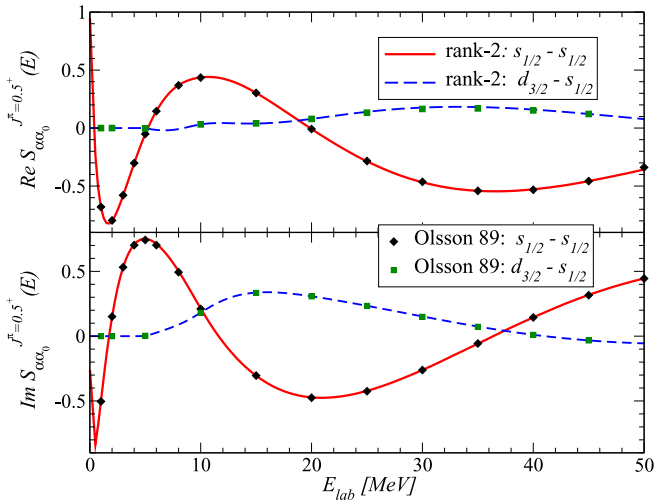

FIG. 1. The energy-dependent EST (eEST) separable representation of the $J^\pi = 1/2^+$ multichannel S-matrix elements, $S^J_{\alpha\alpha_0}(E)$, for the $n + {}^{12}$C system as function of the laboratory energy. The solid (dashed) line represents the S-matrix elements obtained with a rank-2 eEST separable representation in the $0^+ \otimes s_{1/2} \to 0^+ \otimes s_{1/2}$ ($0^+ \otimes s_{1/2} \to 2^+ \otimes d_{3/2}$) channel. The support points are located at 6 and 40 MeV. The filled diamonds and squares represent the corresponding S-matrix elements directly evaluated with the Olsson DOMP [28].

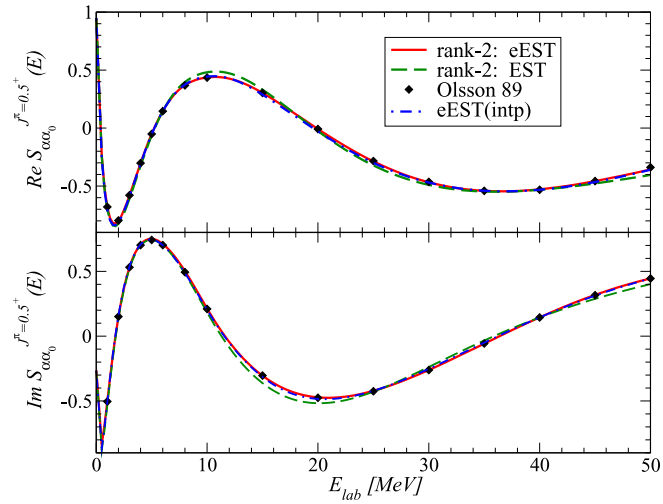

FIG. 2. The S-matrix elements of the $0^+ \otimes s_{1/2} \to 0^+ \otimes s_{1/2}$ channel for the $n + {}^{12}$C system as function of the laboratory energy. The solid line represent the rank-2 energy-dependent eEST separable representation, while the dashed line give the energy-independent EST separable representation. For both, the support points are at 6 and 40 MeV. The dash-dotted line shows the S-matrix elements obtained with the interpolated eEST scheme. The filled diamonds represent the calculation based directly on the Olsson DOMP [28].

must be treated with a coupled-channel formalism. Further details about the model are provided in Appendix C. The Olsson DOMP only considers elastic scattering and inelastic scattering to the first excited state.

First, we construct a separable representation of the Olsson DOMP using the multichannel eEST scheme. Then the corresponding separable t matrix, the S matrix, and the differential cross sections are computed. They agree very well with those obtained by directly solving Eq. (5) with the Olsson DOMP. Finally, by considering the off-shell t matrix elements, we illustrate that the multichannel eEST separable representation of the DOMP obeys the reciprocity theorem.

1. S-matrix elements and differential cross section

First, we want to consider S-matrix elements in well-defined channels to study how well the energy-dependent multichannel eEST scheme can represent them and what rank is required to do so. In Fig. 1, the $J^\pi = 1/2^+$ S-matrix elements, $S^J_{\alpha\alpha_0}(E)$, are shown for the $0^+ \otimes s_{1/2} \to 0^+ \otimes s_{1/2}$ and $0^+ \otimes s_{1/2} \to 2^+ \otimes d_{3/2}$ channels for neutron scattering from ^{12}C as function of the laboratory energy. The diagonal $0^+ \otimes s_{1/2} \to 0^+ \otimes s_{1/2}$ channel is represented by the solid line and the coupling to the $2^+ \otimes d_{3/2}$ by the dashed line. The corresponding S matrix elements obtained by directly solving Eq. (5) with the Olsson DOMP are represented by the solid diamonds and squares. The agreement between the energy-dependent separable representation and the original calculation is excellent. It should be noted that in this case already a rank-2 representation with support points at 6 and 40 MeV is sufficient to achieve this high-quality agreement between 0 and 50 MeV laboratory energy.

The energy-independent EST scheme is a simplification of the eEST scheme leading to an energy-independent separable representation. To illustrate the difference between the two schemes, Fig. 2 shows the S-matrix elements in the diagonal channel $0^+ \otimes s_{1/2} \longrightarrow 0^+ \otimes s_{1/2}$ computed in the eEST scheme (solid line) and the energy-independent EST scheme (dashed line) using the same support points (rank). As a reference, the results obtained by solving Eq. (5) with the original multichannel Olsson optical potential are given by the filled diamonds. The figure clearly shows that the representation with the EST scheme is of lesser quality than the eEST scheme. This finding is consistent with observations for representations of single-channel optical potentials [18]. This suggests that the EST scheme might be improved by increasing the rank of the representation. However, in the multichannel case there is an additional complication, since in the energy-independent scheme coupling matrix elements are not symmetric, i.e., $S^J_{\alpha\alpha'} \neq S^J_{\alpha'\alpha}$, as will be illustrated later.

The numerical effort needed to evaluate the matrix elements $\mathcal{U}^{e,\alpha\beta}_{ij}(E)$ increases rapidly with the number of coupled channels. To simplify the implementation of the eEST scheme, one can avoid the evaluation of these matrix elements for every energy one wants to compute. Instead, $\mathcal{U}^{e,\alpha\beta}_{ij}(E)$ can be computed at fixed energies and an interpolation scheme used to determine its value elsewhere. Following Ref. [19], we choose the fixed energies to coincide with the EST support points. Such a choice has the advantage that the potential matrix elements are needed only at the support points. The results obtained with the interpolated eEST scheme are shown by the dash-dotted lines in Fig. 2. We observe that

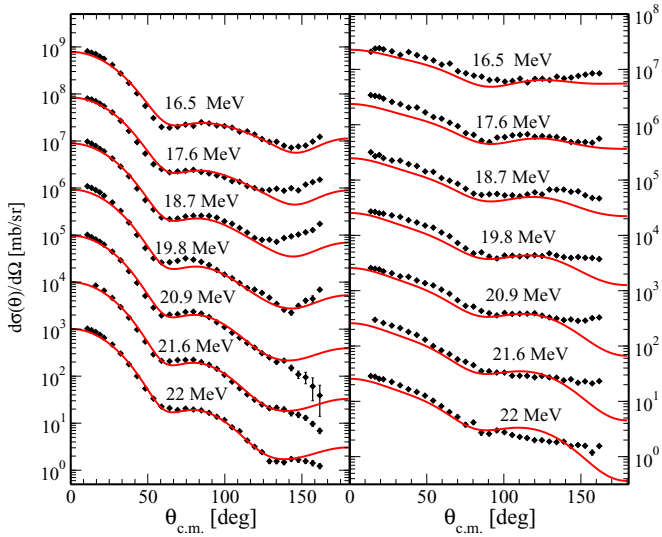

FIG. 3. The differential cross sections for scattering in the $n + {}^{12}$C system computed at different incident neutron energies with the eEST separable representation of the Olsson DOMP [28] (solid lines). The left-hand panel shows the differential cross section for elastic scattering, while the right-hand panel depicts the differential cross section for inelastic scattering to the 2^+ state of ^{12}C. The filled diamonds represent the data taken from Ref. [28]. The cross sections are scaled up by multiples of 10. The results at 21.6 MeV are multiplied by 10, those at 20.9 are multiplied by 100, etc.

the results agree remarkably well with those obtained with the exact eEST scheme. To show the overall quality of the eEST separable representation in all partial-wave S-matrix elements, we compute cross sections for elastic and inelastic scattering. In Fig. 3, the differential cross sections for elastic and inelastic scattering for the $n + {}^{12}$C system are shown at various incident neutron energies. The left-hand panel shows the differential cross section for elastic scattering, and the right-hand panel shows the differential cross section for inelastic scattering to the 2^+ state of ^{12}C. The support points are at $E_{\rm lab} = 6$ and 40 MeV. The separable representation describes both differential cross sections very well and agrees with the coupled-channel calculation directly based on the Olsson potential. However, we want to point out that the angular region beyond about 120 deg of both experimental differential cross sections is not well described by the Olsson DOMP. This may be due to omitting additional excited states or not taking into account rearrangement channels.

2. *Off-shell t matrices*

The reciprocity theorem requires that the off-shell t matrix be invariant under simultaneous interchange of channel indices and momenta. It is thus imperative that we investigate the properties of the off-shell t matrix elements computed with the separable representation schemes. First, we calculate the multichannel off-shell t matrix with the original Olsson DOMP and show the real parts of the $J^\pi = 1/2^+$ t matrix for the $n + {}^{12}$C system at 20.9 MeV incident neutron energy in Fig. 4. The matrix elements correspond to the quantum numbers $\alpha_0 = \{I = 0,\ l = 0,\ j = 0.5\}$ and $\alpha_1 = \{I = 2,\ l = 2,\ j = 3/2\}$. We observe that the t matrices exhibit high momentum components in all channels, which is characteristic of local potentials. In the coupled channels, they are invariant under the simultaneous interchange of channel indices and momenta, as required by the reciprocity theorem.

Next, we explore the off-shell properties of t matrix obtained with the eEST separable representation scheme. In

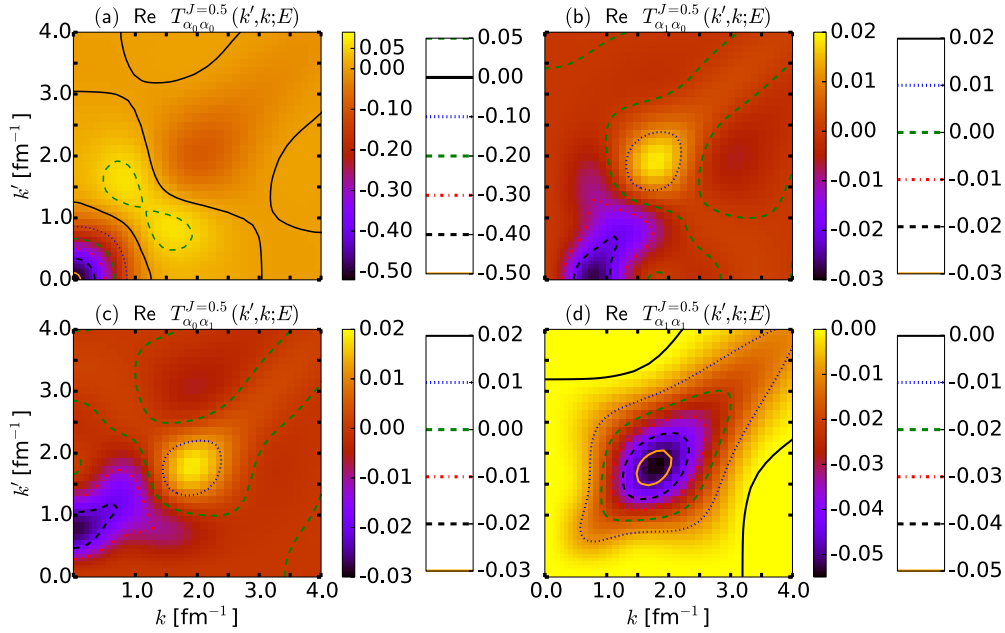

FIG. 4. The real part of the t matrix elements for $J^\pi = 1/2^+$ in the $n + {}^{12}$C system at 20.9 MeV incident neutron energy. Panels (a), (b), (c), and (d) depict $T_{\alpha_0\alpha_0}$, $T_{\alpha_1\alpha_0}$, $T_{\alpha_0\alpha_1}$, and $T_{\alpha_1\alpha_1}$. The quantum numbers for the channels shown here are $\alpha_0 = \{I = 0,\ l = 0,\ j_p = 1/2\}$ and $\alpha_1 = \{I = 2,\ l = 2,\ j_p = 1.5\}$. The on-shell momentum is given by $k_0 = 0.93$ fm^{-1}.

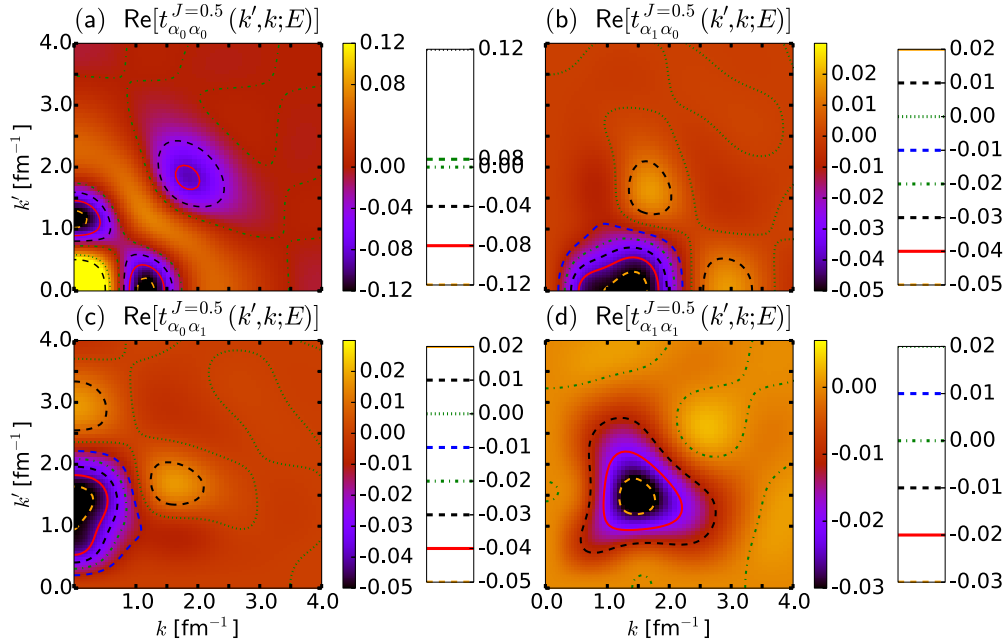

FIG. 5. The real part of multichannel off-shell eEST separable t matrix elements for the $n + {}^{12}$C system at 20.9 MeV incident neutron energy. Panels (a), (b), (c), and (d) depict $T_{\alpha_0\alpha_0}$, $T_{\alpha_1\alpha_0}$, $T_{\alpha_0\alpha_1}$, and $T_{\alpha_1\alpha_1}$. The quantum numbers for the states shown here are $J^\pi = 1/2^+$ $\alpha_0 = \{I = 0,\ l = 0,\ j = 0.5\}$, and $\alpha_1 = \{I = 2,\ l = 2,\ j = 1.5\}$. The on-shell momentum is given by $k_0 = 0.93$ fm^{-1}.

Fig. 5, the real part of the multichannel eEST separable t matrix is shown for the $n + {}^{12}$C system at 20.9 MeV incident neutron energy for the same channels. First, we observe that the separable representation does not contain high-momentum components in either channel. We also see that t-matrix elements obtained with the eEST separable representation are invariant under a simultaneous interchange of channel indices and momenta, as required by the reciprocity theorem. To illustrate that the energy-independent EST separable representation is deficient in that respect, Fig. 6 shows the off-shell t matrix for the same channels. It is quite obvious that the channel-coupling t matrices, Figs. 6(b) and 6(c), are not invariant under a simultaneous interchange of channel indices and momenta. However, even the diagonal channels, Figs. 6(a) and 6(d), are not symmetric under the exchange of k and k'. This violation was already found for single-channel energy-independent EST calculations [19]. In multichannel calculations, this violation of symmetry seems to be enhanced.

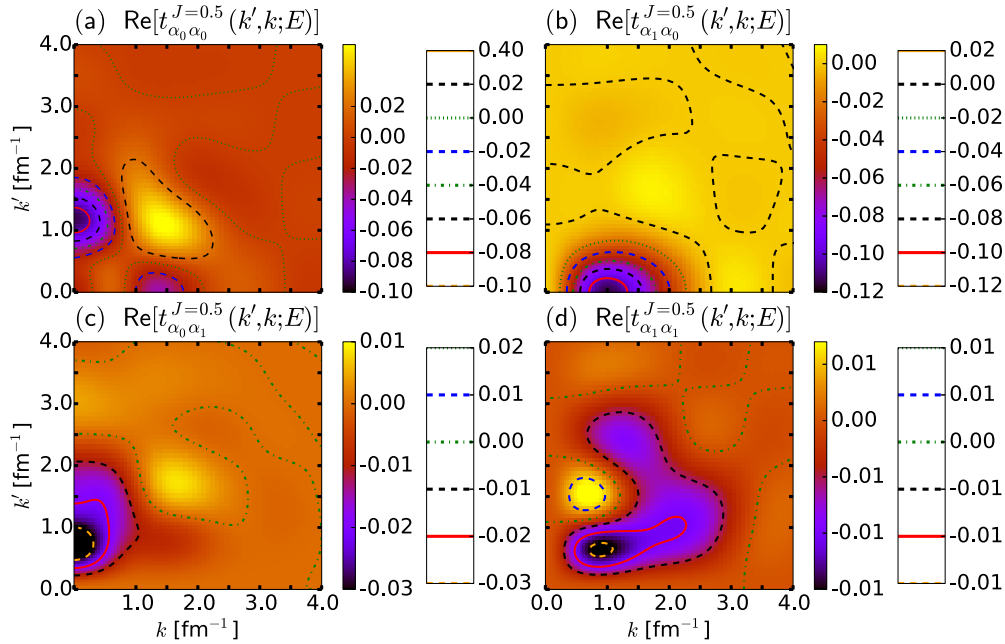

FIG. 6. Same as Fig. 8 but for the EST separable representation of the t matrix.

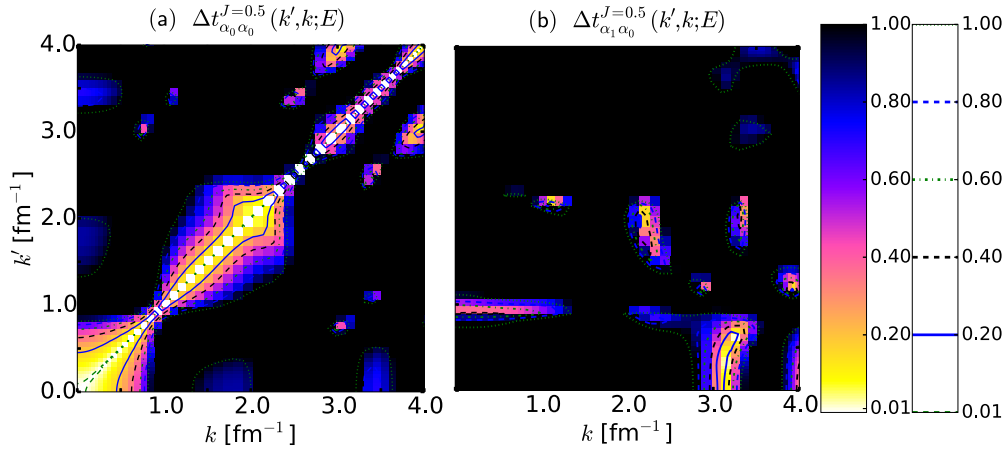

FIG. 7. The $J^\pi = 1/2^+$ asymmetry for the $n + {}^{12}$C system evaluated at 20.9 MeV as function of the off-shell momenta k' and k. Panels (a)and (b) show the asymmetry for the energy-independent EST separable representations.

To determine the extent to which reciprocity is violated (as in Ref. [19]), we define an asymmetry relation as

$$\Delta t^J_{\alpha\alpha_0}(k',k;E) = \left| \frac{t^J_{\alpha\alpha_0}(k',k;E) - t^J_{\alpha_0\alpha}(k,k';E)}{[t^J_{\alpha\alpha_0}(k',k;E) + t^J_{\alpha_0\alpha}(k,k';E)]/2} \right|. \quad (28)$$

In Fig. 7, this asymmetry is shown for the $n + {}^{12}$C system computed at 20.9 MeV as a function of the off-shell momenta k' and k for the energy-independent EST representation. Figure 7(b) clearly shows that even at the on-shell point ($k' = k = k_0 = 0.93$ fm^{-1}) the asymmetry in the $\alpha \neq \alpha_0$ channel is nonzero. This behavior cannot be repaired by increasing the rank of the separable representation. The same calculation for the eEST representation will give exactly zero for all values of k' and k in all channels. The panels would be white and are therefore not shown. From this, we conclude that for a separable representation of energy-dependent multichannel complex optical potential, the eEST scheme must be applied if reciprocity should be fulfilled.

III. SEPARABLE REPRESENTATION OF ENERGY-DEPENDENT MULTICHANNEL PROTON-NUCLEUS OPTICAL POTENTIALS

A. Formal considerations

The interaction of protons with nuclei comprises the strong nuclear force and the Coulomb potential. The nuclear interaction is given by the complex, energy-dependent optical potential and usually has the same form as the neutron optical potential. The Coulomb interaction consists of a long-ranged point-Coulomb potential V^C and a short-ranged piece. The latter arises from the charge distribution of the nucleus and is commonly approximated by a uniformly charged sphere. The point-Coulomb potential is long ranged and affects the asymptotic behavior of the scattering wave functions. Consequently, the proton-nucleus scattering problem cannot be treated with the same techniques employed for neutron scattering in Sec. II. According to the Goldberger-Gell-Mann relation [29], the scattering amplitude for $p + A$ scattering separates into two parts. The first part is the Rutherford amplitude corresponding to the point Coulomb potential. The second part is the nuclear amplitude corresponding to the short-range potential U, consisting of the nuclear interaction and the short-range Coulomb potential. While the Rutherford amplitude is known analytically, the nuclear amplitude must be evaluated numerically. The nuclear amplitude is evaluated in a basis of Coulomb wave functions according to Eq. (A14). When working in momentum space, this is a very challenging task since the Coulomb wave functions are singular. We employ the techniques presented in Ref. [30], where the authors showed that, in the Coulomb basis, the Coulomb-distorted nuclear t matrix fulfills a LS-type equation of the same form as in the basis of plane waves. The momentum-space matrix elements of the potential in the Coulomb basis are obtained via Fourier transform from coordinate space. For multichannel potentials, the nuclear t matrix fulfills the coupled set of LS-type equations shown in Eq. (B7).

To derive a separable representation for the short-ranged proton-nucleus potential U, we modify the multichannel eEST scheme of Sec. II A 2. The multichannel scattering wave functions $|\Psi^{(+)}_{\rho,i}\rangle$ are replaced by the Coulomb-distorted multichannel scattering wave functions $|\Psi^{c(+)}_{\rho,i}\rangle$. This leads to the separable potential

$$\begin{aligned} u(E) &= \sum_{\rho\sigma}\sum_{ij} U(E_i)\left|\Psi^{c(+)}_{\gamma\rho,i}\right\rangle \lambda^{c,\,\rho\sigma}_{ij}(E)\left\langle\Psi^{c(-)}_{\sigma,j}\right|U(E_j), \\ &= \sum_{\rho\sigma}\sum_{ij} T^c(E_i)\left|\rho\ \phi^{c\rho}_i\right\rangle \lambda^{c,\,\rho\sigma}_{ij}(E)\left\langle\phi^{c\sigma}_j\ \sigma\right|T^c(E_j). \end{aligned} \quad (29)$$

Here $\phi^{c\sigma}_j$ are the scattering Coulomb wave functions corresponding to the channel momentum k^σ_j. The Coulomb-distorted nuclear transition matrix $T^c(E)$ fulfills the LS equation

$$T^c(E) = U + UG_C(E)T^c(E), \quad (30)$$

with $G_C(E) = [E - H_0 - V^C + i\epsilon]^{-1}$ being the Coulomb Green's function, H_0 being the free Hamiltonian, and V^C being the point-Coulomb potential. In analogy to Eqs. (14) and (15),

we define the energy-dependent matrix

$$\mathcal{U}^{e,\alpha\beta}_{mn}(E) \equiv \langle \Psi^{c(-)}_{\alpha,m} | U(E) | \Psi^{c(+)}_{\beta,n} \rangle, \tag{31}$$

and the energy-independent matrix

$$\mathcal{U}^{c\alpha\beta}_{mn} = \mathcal{U}^{ce,\alpha\beta}_{mn}(E_m) \equiv \langle \Psi^{c(-)}_{\alpha,m} | U(E_m) | \Psi^{c(+)}_{\beta,n} \rangle. \tag{32}$$

The coupling matrix elements $\lambda^{c,\,\rho\sigma}_{ij}(E)$ then fulfill

$$\begin{aligned}\mathcal{U}^{ce,\alpha\beta}_{mn}(E) &\equiv \langle \Psi^{c(-)}_{\alpha,m} | u(E)\ \Psi^{c(+)}_{\beta,n} \rangle, \\ &= \sum_{\rho\sigma}\sum_{ij} \langle \Psi^{c(-)}_{\alpha,m} | T^c(E_i) | \rho J M\ \phi^{c\rho}_i \rangle\ \lambda^{c,\,\rho\sigma}_{ij}(E) \\ &\quad \times \langle \phi^{c\sigma}_j | T^c(E_j) | \Psi^{c(+)}_{\nu\beta,n} \rangle, \\ &= [\mathcal{U}^{ct} \cdot \lambda^c(E) \cdot \mathcal{U}^c]^{\alpha\beta}_{mn}. \end{aligned} \tag{33}$$

Here $\mathcal{U}^{ct}$ represents the transpose of $\mathcal{U}^c$. The separable representation of the t matrix is then given as

$$\begin{aligned} t^c(E) &= \sum_{\rho\sigma}\sum_{ij} U(E_i) | \Psi^{c(+)}_{\rho,i} \rangle\ \tau^{c,\,\rho\sigma}_{ij}(E)\ \langle \Psi^{c(-)}_{\sigma,j} | U(E_j), \\ &= \sum_{\rho\sigma}\sum_{ij} T^c(E_i) | \rho \phi^{c\rho}_i \rangle\ \tau^{c,\,\rho\sigma}_{ij}(E)\ \langle \phi^{c\sigma}_j\ \sigma | T^c(E_j). \end{aligned} \tag{34}$$

Substituting Eqs. (29)–(34) into the LS equation leads to

$$R^c(E) \cdot \tau^c(E) \cdot \mathcal{U}^c = \mathcal{U}^{ce}(E), \tag{35}$$

where

$$\begin{aligned} R^{c,\,\rho\sigma}_{ij}(E) &= \langle \phi^{c\rho}_i | T^c_{\rho\sigma}(E_i) + \sum_{\beta} T^c_{\rho\beta}(E_i) G_{C\beta}(E_j)\ T^c_{\beta\sigma}(E_j) \\ &\quad \times | \phi^{c\sigma}_j \rangle - \sum_{\beta\beta'}\sum_{n} \mathcal{M}^{c,\,\rho\beta}_{in}(E) \\ &\quad \times \langle \phi^{c\beta}_n | T^c_{\beta\beta'}(E_n) G_{C\beta'}(E) T^c_{\beta'\sigma}(E_j) | \phi^{c\sigma}_j \rangle \end{aligned} \tag{36}$$

and

$$\mathcal{M}^{c,\,\rho\sigma}_{ij}(E) = [\mathcal{U}^{ce}(E) \cdot (\mathcal{U}^c)^{-1}]^{\rho\sigma}_{ij}. \tag{37}$$

Here, the indices β, β' represent angular momentum channels. It is noteworthy that the expressions for the Coulomb distorted separable multichannel nuclear t matrix elements have the same form as the ones obtained for neutron-nucleus systems in Sec. II A 2. The only difference is that all quantities are evaluated in the Coulomb basis. Moreover, the behavior of the off-shell nuclear t matrices under a transposition does not depend on the chosen basis, and thus the multichannel eEST separable representation for proton-nucleus systems fulfills the reciprocity in the same fashion as the one for neutron-nucleus systems.

B. Elastic and inelastic scattering of protons from ^{12}C

To illustrate the implementation of the multichannel separable expansion presented in Sec. III A, we consider the scattering of protons from ^{12}C including both the the 0^+ ground state and 2^+ excited state. A rigid rotor model is adopted to describe the structure of the ^{12}C nucleus as in Sec. II B. The proton-^{12}C interaction is given by a deformed OMP plus the point-Coulomb potential. The proton OMP includes a short-range contribution arising from the nuclear charge distribution. Deformations are introduced using multipole expansions as outlined in Appendix C. In this work, we employ the Meigooni [31] DOMP, which is presented in Appendix C 2. A uniformly charged sphere is assumed for the nuclear charge distribution so that the short-ranged Coulomb potential has the form

$$V_{\rm coul}(r, R_c) = Z\alpha \left[\frac{1}{2R_c}\left(3 - r^2/R_c^2\right) - \frac{1}{r} \right]. \tag{38}$$

The values of the Coulomb radius R_c are adopted from Ref. [32]. Here, Z is the atomic number and α is the electromagnetic coupling constant.

First, the differential cross sections are evaluated using the Meigooni DOMP and compared to the ones obtained using its separable representation. In Fig. 8, the differential cross section for elastic proton scattering from ^{12}C as function of the center of mass (c.m.) angle $\theta_{c.m.}$ is shown for proton incident energies at 35.2 MeV [Fig. 8(a)] and 65 MeV [Fig. 8(c)]. The solid lines show the eEST separable representation while the crosses represent calculations based on the original Meigooni DOMP. The support points for the separable representation are chosen to be at $E_{\rm lab} = 25$, 45, and 65 MeV. The differential cross sections for inelastic scattering to the 2^+ state are shown in Figs. 8(b) and 8(d) for the same energies. We observe that the cross sections computed with the eEST separable representation of rank 3 agree very well with the ones computed directly from the Meigooni DOMP.

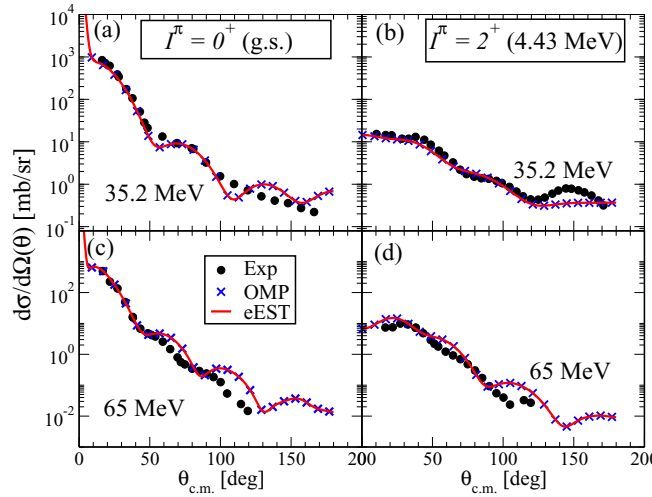

FIG. 8. The differential cross sections for proton scattering off ^{12}C. Panels (a) and (c) depict the differential cross sections for elastic scattering at proton incident energies of 35.2 MeV (a) and 65 MeV (c). The corresponding cross sections for inelastic scattering to the 2^+ state at 4.43 MeV are depicted in panels (b) and (d). The solid lines represent the calculations with the eEST separable representation, while calculations with the original optical potential by Meigooni [31] are given by the crosses. The support points for the separable representation at located at $E_{\rm lab} = 25$, 45, and 65 MeV. The data represented by filled circles at 35 and 65 MeV are taken from Refs. [33] and [34] respectively.

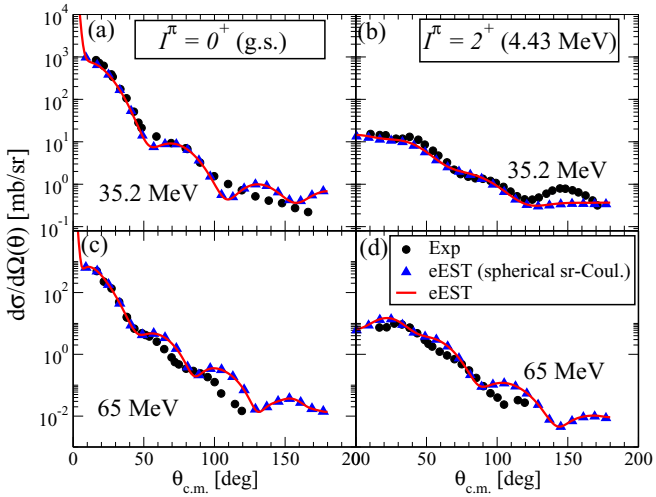

FIG. 9. The differential cross sections for proton scattering off ^{12}C. Panels (a) and (c) depict the differential cross sections for elastic scattering at proton incident energies of 35.2 MeV (a) and 65 MeV (c). The corresponding cross sections for inelastic scattering to the 2^+ state at 4.43 MeV are depicted in panels (b) and (d). The solid lines represent the calculations with the eEST separable representation. The support points for the separable representation at located at $E_{\rm lab} = 25, 45$, and 65 MeV. The filled triangles represent a calculation in which only the short range nuclear potential is deformed, while the short-ranged Coulomb potential spherical. The data at 35 and 65 MeV are taken from Refs. [33] and [34] respectively.

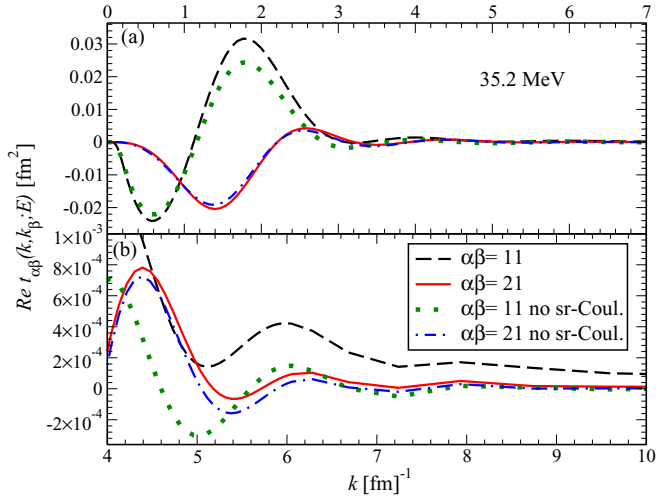

FIG. 10. The real part of half-shell multichannel t matrix elements $t^{J^\pi}_{\alpha 1}(k,k_1;E)$ for $J^\pi = 1/2^+$ for proton scattering from ^{12}C at incident proton energy 35.2 MeV. Panel (a) shows the half-shell t matrix in the interval $0\ {\rm fm}^{-1} \leqslant k \leqslant 7\ {\rm fm}^{-1}$, while panel (b) depicts the same half-shell t matrix between $k = 4$ and $10\ {\rm fm}^{-1}$. The channels 1 and 2 are represented as $1 \equiv \{I = 0,\ l = 0,\ j = 1/2\}$ and $2 \equiv \{I = 0,\ l = 2,\ j = 3/2\}$. The dashed line represents the t matrix elements $t^{1/2^+}_{11}(k,k_1;E)$ calculated from the eEST separable representation of the Meigooni DOMP [31] for the on-shell momentum $k_1 = 1.2\ {\rm fm}^{-1}$ as function of k. The solid line gives the t matrix elements $t^{1/2^+}_{21}(k,k_1;E)$ obtained in the same fashion, but multiplied by a factor of 3 to enhance its features. For the calculations of the same channels, represented with the dotted and dash-dotted lines, the short-ranged Coulomb potential is omitted.

When incorporating the rotational excitation of ^{12}C in the calculations presented in Fig. 8, we deformed the nuclear part of the optical potential as well as the short-ranged Coulomb potential, since the charge distribution should undergo the same deformation as the nuclear short-ranged potential. In order to investigate if deforming the short-ranged Coulomb potential affects the cross sections, we carry out the same calculations as before, but keeping the short-range Coulomb potential spherical. The result of this calculation is shown in Fig. 9 by the filled upward triangles. It is interesting to note that the differential cross sections for inelastic scattering do not show any effect of this simplification. This may be due to the still relatively small charge ($Z = 6$) of ^{12}C where a deviation from a spherical charge has a small effect. In the framework of (d,p) reactions on ^{24}Mg it was shown that for $Z = 12$ the deformation of the charge only leads to a very small effect in the transfer cross section [14]; thus our finding is consistent. However, since the strength of the short-ranged Coulomb force depends on nuclear charge, its deformation would have a larger effect on the cross sections for heavier nuclei.

Differential cross sections are summed up over all partial waves. The fact that the eEST scheme represents the cross sections directly obtained from the Meigooni DOMP very well implies that overall the partial waves must be well represented. To study further details, we now concentrate on the $J^\pi = 1/2^+$ state and study the half-t matrices $t^{J^\pi}_{\alpha,1}(k,k_1;E)$ calculated at the incident proton energy 35.2 MeV in more detail. Here, α can take the values $\alpha = 1 = \{I = 0,\ l = 0,\ j = 1/2\}$ and $\alpha = 2 = \{I = 0,\ l = 2,\ j = 3/2\}$. The real parts of the t matrices in those channels are depicted in Fig. 10. Figure 10(a) shows the half-shell t matrix elements for the channels 11 and 21 in the interval $0\ {\rm fm}^{-1} \leqslant k \leqslant 7\ {\rm fm}^{-1}$ for the full calculation and a calculation in which the short-range Coulomb potential is omitted. The matrix elements in the 21 channel are multiplied with a factor 3 to be roughly of the same size as the matrix elements in the 11 channel. Since the fall-off behavior of the matrix elements for large momenta may be important for reaction calculations, we depict in Fig. 10(b) the matrix elements in the momentum interval $4\ {\rm fm}^{-1} \leqslant k \leqslant 10\ {\rm fm}^{-1}$. Here, we see that the short-range Coulomb potential mainly influences the diagonal 11 channel. At $6\ {\rm fm}^{-1}$, the t matrix calculated with the nuclear potential only is essentially zero, while the short-ranged Coulomb potential still gives a small contribution. In the 21 channel, both t matrices fall off to zero, indicating that the deformation of the short-ranged Coulomb potential has little effect for a nucleus as light as ^{12}C. This may, however, be different when considering heavier nuclei and will have to be investigated further.

Finally, we separately investigate the effects of the deformation of the short-ranged Coulomb potential on the half-shell multichannel t matrix elements. To do so, the coupled-channel calculation is carried out with a spherical short-ranged Coulomb potential and compared with the full calculation. This comparison is shown in Fig. 11. We plot the t matrices in the same momentum ranges as in Fig. 10.

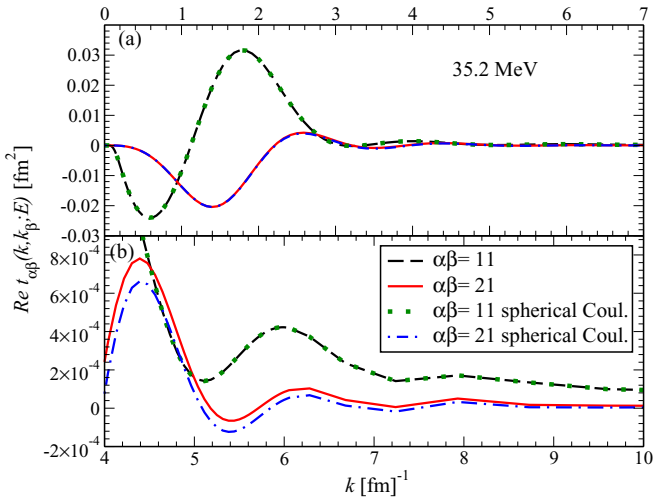

FIG. 11. Same as Fig. 10. However, for the calculations represented with the dotted and dash-dotted lines, the short-ranged Coulomb potential is included but taken to be spherical. The t-matrix elements of the coupling channels are multiplied by a factor 3 to enhance their features.

In the curves in Fig. 11(a), we cannot discern between the two calculations. Only when considering a much smaller scale in Fig. 11(b) are the calculations in the 21 channel slightly different. However, the differences are so small that using a spherical short-range Coulomb potential can be considered a good approximation for ^{12}C, as already seen in the cross section at high momentum transfer in Fig. 9.

IV. SUMMARY AND CONCLUSION

In this work, we introduce separable representations of complex, energy-dependent multichannel optical potentials for neutron as well as proton scattering from nuclei. To fulfill reciprocity exactly, the separable representation must be energy dependent. This is achieved by having energy-dependent coupling constants.

The first part of the paper concentrates on the separable expansion of neutron-nucleus deformed optical model potentials (DOMPs). This is achieved by generalizing the energy-dependent EST (eEST) scheme of Ref. [19] to multichannel potentials. To illustrate the implementation of the multichannel eEST scheme, we considered neutron scattering from ^{12}C. In order to describe the structure of the ^{12}C nucleus, the rigid rotor model is assumed, and the Olsson [28] DOMP was adopted to describe the effective neutron-^{12}C interaction. The multichannel eEST scheme was then used to construct a separable representation for the Olsson DOMP. In this case, a rank-2 separable expansion was sufficient to describe elastic and inelastic scattering cross sections between 0 and 50 MeV incident neutron energies.

To demonstrate the necessity of using an energy-dependent multichannel separable representation, we also constructed a separable expansion based on the energy-independent multichannel EST scheme, which needed to be of rank 3 to match the representation of S-matrix elements between 0 and 50 MeV with the same quality as the eEST scheme. An examination of the off-shell t matrix elements showed that only the multichannel eEST separable representation fulfills reciprocity; i.e., the t matrix is invariant upon a simultaneous interchange of momenta and channel indices. In contrast, the energy-independent multichannel expansion yields an asymmetric off-shell t matrix, as was already observed in single-channel expansions in Ref. [19].

The cost of implementing the eEST scheme for multichannel potentials increases with the number of channels, since the matrix elements $\mathcal{U}_{ij}^{e,\alpha\beta}(E)$ must be calculated at each desired energy E. However, it turns out that it is sufficient to compute this matrix element at fixed energies and interpolate on the energy to obtain its value at arbitrary energies. As already observed in Ref. [19] for single-channel potentials, the results obtained with the interpolated eEST scheme agree very well with the ones obtained without the interpolation.

The second part of the paper focuses on the separable representation of proton-nucleus DOMPs. The proton-nucleus potential consists of a nuclear piece as well as the Coulomb interaction. The Coulomb interaction further separates into a short-ranged part, usually represented as a charged sphere, and a long-ranged point-Coulomb force. The point-Coulomb potential is incorporated by working in the Coulomb basis in accordance with the Gell-Mann-Goldberger [29] relation. In order to employ the eEST scheme in the same fashion as for neutron-nucleus scattering, we need to solve a Lippmann-Schwinger type equation to obtain half-shell t matrices in the Coulomb basis. While the Coulomb propagator is quite simple in this basis, the evaluation of potential matrix elements is more involved. We followed Ref. [30] to evaluate the potential matrix elements.

To demonstrate an implementation of an eEST representation of a proton-nucleus optical potential, we considered proton scattering off ^{12}C and used the Meigooni [31] DOMP as a starting point. Differential cross sections for elastic and inelastic scattering were computed using the eEST scheme, showing that a rank-3 separable expansion is sufficient to represent the Meigooni [31] DOMP. Note that the only difference between the eEST schemes for neutron and proton optical potentials is the basis employed for the separable expansion. This implies that the discussions on reciprocity given in Sec. II B for neutron-nucleus potentials apply to proton-nucleus systems as well.

In the Meigooni DOMP, the short-ranged Coulomb potential is deformed in the same fashion as the short-range nuclear potential. To study the effects of deforming the short-ranged Coulomb potential, the coupled-channel calculations were repeated with the Coulomb deformation parameter set to zero. It was observed that the differential cross sections are not significantly altered by using a spherical short-ranged Coulomb potential. The effect on the half-shell t matrix elements for elastic scattering is also negligible. There is a minimal change to the half-shell t matrix elements for inelastic scattering. However, those changes are so small that when considering a nucleus as light as ^{12}C a deformation of the charge distribution may be safely neglected. This insight is consistent with the finding in Ref. [14]. Most likely, for heavier

nuclei this will not be the case and a deformation of the short-ranged Coulomb potential will be mandatory.

ACKNOWLEDGMENTS

This work was performed in part under the auspices of the U.S. Department of Energy under Contract No. DE-FG02-93ER40756 with Ohio University. The authors thank F.M. Nunes for thoughtful comments and careful reading of the manuscript.

APPENDIX A: NUCLEON SCATTERING FROM A DEFORMED NUCLEUS

1. Neutrons

Let us consider a neutron scattering from a nucleus possessing a rotational energy spectrum characterized by the spin-parity I^π. The spectrum corresponds to collective rotational states with wave functions $|\Phi_{IM_I}\rangle$. These are given by [35]

$$\Phi_{IM_IK}(\xi) = \left(\frac{2I+1}{8\pi^2}\right)^{1/2} \mathcal{D}^I_{MK}(\xi), \tag{A1}$$

where $\mathcal{D}^I_{MK}(\xi)$ are the Wigner rotation matrices. Here, ξ are the angles specifying the orientation of the nucleus. The interaction between the neutron and the nucleus leads to couplings between states of different spin parity. Here, we treat couplings to selected rotational states explicitly, while the imaginary part of the optical potential accounts for couplings to all other channels besides those that are included. To compute scattering observables for such systems, the coupled-channels formalism [36] must be adopted.

a. States of conserved angular momentum

To construct states of conserved angular momentum, we adopt the so-called jj-coupling scheme. The neutron spin $s = 1/2$ is coupled to the relative orbital angular momentum l to yield $j_p = |l \pm 1/2|$. The corresponding projections along the z axis m_s and m_l fulfill the condition $m_{j_p} = m_s + m_l$. The angular momentum j_p is in turn coupled to the nuclear spin I to yield the total angular momentum $|I - j_p| \leqslant J \leqslant I + j_p$. The angular momentum J and its projection along the z axis $M = M_I + m_{j_p}$ are conserved. To obtain the states of conserved angular momentum $|(Ilsj_p)JM\rangle$, we first define

$$\left|\mathcal{Y}^{j_p m_{j_p}}_{ls}\right\rangle = \sum_{m_l m_s} C\left(lsj_p, m_l m_s m_{j_p}\right) \left|Y_{lm_l}\right\rangle |sm_s\rangle, \tag{A2}$$

where the functions Y_{lm_l} are the spherical harmonics and χ_{sm_s} is the corresponding spinor. The quantity $C(lsj_p, m_l m_s m_{j_p})$ is the Clebsch-Gordon (CG) coefficient. The inverse relation is given by

$$\left|Y_{lm_l}\right\rangle |sm_s\rangle = \sum_{j_p m_{j_p}} C\left(lsj_p, m_l m_s m_{j_p}\right) \left|\mathcal{Y}^{j_p m_{j_p}}_{ls}\right\rangle. \tag{A3}$$

The sates $|I(lsj_p)JM\rangle$ are constructed by coupling Eq. (A2) to the rotational state $|\Phi_{IM_I}\rangle$ so that

$$|(Ilsj_p)JM\rangle = \sum_{M_I m_{j_p}} C\left(Ij_pJ, M_I m_{j_p} M\right) \left|\mathcal{Y}^{j_p m_{j_p}}_{ls}\right\rangle \left|\Phi_{IM_I}\right\rangle, \tag{A4}$$

with inverse relation

$$\left|\mathcal{Y}^{j_p m_{j_p}}_{ls}\right\rangle \left|\Phi_{IM_I}\right\rangle = \sum_{JM} C\left(Ij_pJ, M_I m_{j_p} M\right) |(Ilsj_p)JM\rangle. \tag{A5}$$

Substituting Eq. (A2) and (A3) into Eqs.(A5) and (A4) leads to

$$|(Ilsj_p)JM\rangle = \sum_{M_I m_{j_p}} \sum_{m_l m_s} C\left(Ij_pJ, M_I m_{j_p} M\right) \times C\left(lsj_p, m_l m_s m_{j_p}\right) \left|Y_{lm_l}\right\rangle |sm_s\rangle \left|\Phi_{IM_I}\right\rangle, \tag{A6}$$

with the inverse relation given by

$$\left|Y_{lm_l}\right\rangle |sm_s\rangle \left|\Phi_{IM_I}\right\rangle = \sum_{JM} \sum_{j_p m_{j_p}} C\left(Ij_pJ, m_I m_{j_p} M\right) \times C\left(lsj_p, m_l m_s m_{j_p}\right) |(Ilsj_p)JM\rangle. \tag{A7}$$

To simplify the notation, we define a channel index $\alpha \equiv (Ilsj_p)$ so that the states of conserved angular momentum can be written as $|(Ilsj_p)JM\rangle = |\alpha JM\rangle$. These states form a complete basis:

$$\mathbf{1} = \sum_{\alpha JM} \alpha JM\rangle\langle\alpha JM|. \tag{A8}$$

b. Scattering amplitudes and cross sections

The on-shell t matrix is related to the S matrix by

$$S^J_{\alpha\alpha_0}(E) = \delta_{\alpha\alpha_0} + 2i\kappa^J_{\alpha\alpha_0}(E),$$
$$\text{with} \quad \kappa^J_{\alpha\alpha_0}(E) = -\pi\sqrt{\rho_\alpha \rho_{\alpha_0}}\, T^J_{\alpha\alpha_0}\left(k^\alpha_0, k^{\alpha_0}_0; E\right). \tag{A9}$$

Here, $\rho_\alpha = \mu_\alpha k^\alpha_0$ is the density of states in channel α. To obtain the scattering amplitude for the process $|\mathbf{k_0} s m_s I M_I\rangle \longrightarrow |\mathbf{k}_\alpha s m'_s I' M'_I\rangle$, we first evaluate the t matrix

$$\begin{aligned} T_{I'M'_I sm'_s : IM_I sm_s}(\mathbf{k}_\alpha, \mathbf{k_0}; E) &= \langle I'M'_I sm'_s \mathbf{k}_\alpha | T(E) | \mathbf{k_0} sm_s IM_I\rangle \\ &= \sum_{JM} \sum_{ll'j_pj'_p} C(Ij_pJ, M_I M - M_I M)\, C(lsj_p, M - M_I - m_s m_s M - M_I) C(l'sj_p, M - M'_I \\ &\quad - m'_s m'_s M - M'_I) C(I'j'_pJ, M'_I M - M'_I M) T^J_{\alpha\alpha_0}(k_\alpha, k_0; E)\; Y_{l'M-M'_I-m'_s}(\hat{\mathbf{k}}_\alpha) Y^*_{lM-M_I-m_s}(\hat{\mathbf{k}}_\mathbf{0}). \end{aligned} \tag{A10}$$

The scattering amplitude for can be inferred from the relation [37]

$$f_{I'M_I'sm_s':IM_Ism_s}(E,\theta) = \langle I'M_I'sm_s'\mathbf{k}_\alpha|f(E)|\mathbf{k_0}sm_sIM_I\rangle = \frac{4\pi^2}{k_0}\sqrt{\rho_{\alpha_0}\rho_\alpha}\langle I'M_I'sm_s'\mathbf{k}_\alpha|T(E)|\mathbf{k_0}sm_sIM_I\rangle. \tag{A11}$$

If the momentum $\mathbf{k_0}$ is chosen to be along the z axis, the orbital angular momentum l has no projection along this direction. Since we are dealing with axially symmetric potentials, we set the azimuthal angle $\phi = 0$. The scattering amplitude thus takes the form

$$\begin{aligned} f_{I'M_I'sm_s':IM_Ism_s}(E,\theta) = \frac{4\pi}{k_0}\sum_{JM}\sum_{ll'j_pj_p'} & C(Ij_pJ,M_IM-M_IM)\,C(lsj_p,M-M_I-m_sm_sM-M_I) \\ & \times C(l'sj_p,M-M_I'-m_s'm_s'M-M_I')\,C(I'j_p'J,M_I'M-M_I'M)\kappa^J_{\alpha\alpha_0}(E)\,Y_{l'M-M_I'-m_s'}(\theta,0)Y^*_{l0}(0,0). \end{aligned} \tag{A12}$$

Finally, to obtain the differential cross section, we take the square of the scattering amplitude $|f_{I'M_I'sm_s':IM_Ism_s}(E,\theta)|^2$. If the spin projections are not measured, the cross section is evaluated by averaging over the initial magnetic quantum numbers and summing over the final ones. This leads to the unpolarized differential cross section

$$\frac{d\sigma(\theta)}{d\Omega} = \frac{1}{(2I+1)(2s+1)}\sum_{M_I'm_{s'}}\sum_{M_Im_s}\left|f_{I'M_I'sm_{s'}:IM_Ism_s}(E,\theta)\right|^2. \tag{A13}$$

2. Protons

The coupled-channel calculations for proton-nucleus systems proceed similarly to those of the neutron-nucleus systems. However, due to the presence of the Coulomb force, the point-Coulomb is separated via the Gell-Mann-Golberger relation [29] and the nuclear amplitude is calculated in the basis of Coulomb scattering states. The full proton-nucleus scattering amplitude thus takes the form [27]

$$\begin{aligned} f_{I'M_I'sm_s':IM_Ism_s}(E,\theta) = f_c(\theta)\delta_{I'M_I'sm_s':IM_Ism_s} + \frac{4\pi}{k_0}\sum_{JM}\sum_{ll'j_pj_p'} & e^{i[\sigma_{l'}(k_\alpha)+\sigma_l(k_0)]}C(Ij_pJ,M_IM-M_IM) \\ & \times C(lsj_p,M-M_I-m_sm_sM-M_I)C(l'sj_p,M-M_I'-m_s'm_s'M-M_I') \\ & \times C(I'j_p'J,M_I'M-M_I'M)\kappa^{cJ}_{\alpha\alpha_0}(E)\,Y_{l'M-M_I'-m_s'}(\theta,0)Y^*_{l0}(0,0). \end{aligned} \tag{A14}$$

Here, $f_c(\theta)$ is the Rutherford amplitude and $\sigma_{l'}(k_0)$ is the Coulomb phase shift. The dimensionless $\kappa^{cJ}_{\alpha\alpha_0}(E)$ is related to the Coulomb-distorted multichannel t matrix $T^{cJ}_{\alpha\alpha_0}(k_0^\alpha,k_0^{\alpha_0};E)$ by Eq. (A9). The unpolarized differential cross sections computed are according to Eq. (A13).

APPENDIX B: NUMERICAL ASPECTS

1. Neutron optical potentials

To evaluate the separable t matrix of Eq. (17), the multichannel half-shell t matrices $T^J_{\alpha\rho}(E_i)|k_i^\rho\rangle$ and coupling matrix $\tau^{\rho\sigma}_{ij}(E)$ are required as input. The half-shell t matrices are obtained as solutions of Eq. (5). The matrix $\tau^{\rho\sigma}_{ij}(E)$ is determined by solving Eq. (18), where the matrix $R^{\rho\sigma}_{ij}(E)$ is calculated according to Eq. (19). For the purpose of evaluating $\tau^{\rho\sigma}_{ij}(E)$ numerically, a different notation for the channel and energy indices is adopted. Each combination $\{i,\rho\}$ is denoted by a single index a. We proceed by expressing Eqs. (18) and (19) in the form

$$\mathcal{M}_{\rm ab}(E) \equiv [R(E)\cdot\tau(E)]_{\rm ab}, \tag{B1}$$

where

$$R_{\rm ab}(E) = \langle k_a\ aJM|T(E_a)+T(E_a)G_0(E_b)T(E_b)|bJM\ k_b\rangle - \sum_c \mathcal{M}_{\rm ac}(E)\langle k_c\ cJM|T(E_c)G_0(E)T(E_b)|bJM\ k_b\rangle, \tag{B2}$$

with

$$\mathcal{M}_{\rm ac}(E) \equiv [\mathcal{U}^e(E)\mathcal{U}^{-1}]_{\rm ac}. \tag{B3}$$

The explicit momentum space expression for $R(E)$ is given as

$$\begin{aligned} R_{\rm ab}(E) = T^J_{\alpha_a\alpha_b}(k_b,k_a;E_a) + \sum_\beta\int_0^\infty dp\ p^2\ T^J_{\alpha_a,\beta}(p,k_a;E_a)G_{0\beta}(E_b)T^J_{\beta\alpha_b}(p,k_b;E_b) \\ - \sum_c \mathcal{M}_{\rm ac}(E)\sum_\beta\int_0^\infty dp\ p^2\ T^J_{\alpha_c\beta}(p,k_c;E_c)G_{0\beta}(E)T^J_{\beta\alpha_b}(p,k_b;E_b). \end{aligned} \tag{B4}$$

The coupling matrix $\tau(E)$ is thus determined from Eq. (B1) so that the separable multichannel t matrix is given as

$$t^J_{\alpha\beta}(k',k;E) = \sum_{\rho\sigma}\sum_{ij} T^J_{\alpha\rho}\left(k',k^\rho_i;E_i\right)\tau^{\rho\sigma}_{ij}(E)T^J_{\sigma\beta}\left(k,k^\sigma_j;E_j\right),$$
$$= \sum_{\rm ab} T^J_{\alpha a}(k',k_a;E_a)\tau_{\rm ab}(E)T^J_{b\beta}(k,k_b;E_b). \tag{B5}$$

If the potential U is energy independent, the matrix $\mathcal{M}_{\rm ac}(E)$ reduces to an identity matrix. Consequently, the eEST scheme reduces to an energy-independent separable representation. In this limit the matrix $R_{\rm ab}(E)$ is given by

$$R_{\rm ab}(E) = T^J_{\alpha_a\alpha_b}(k_b,k_a;E_a) + \sum_\beta \int_0^\infty dp\ p^2\ T^J_{\alpha_a,\beta}(p,k_a;E_a)G_{0\beta}(E_b)T^J_{\beta\alpha_b}(p,k_b;E_b)$$
$$- \sum_\beta \int_0^\infty dp\ p^2\ T^J_{\alpha_a\beta}(p,k_a;E_a)G_{0\beta}(E)T^J_{\beta\alpha_b}(p,k_b;E_b). \tag{B6}$$

2. Proton-nucleus optical potentials

We note that the separable t matrix given by Eqs. (34)–(36) has a similar form as the one obtained for neutron optical potentials, except that

(a) the half-shell t matrices $T^J_{\alpha\rho}(E_i)|k^\rho_i\rangle$ are replaced by the Coulomb-distorted half-shell t matrices $T^{cJ}_{\alpha\rho}(E_i)|k^\rho_i\rangle$ and
(b) the Coulomb propagator $G_C(E) = [E - H_0 - V^C + i\epsilon]^{-1}$ replaces the free propagator $G_0(E)$.

The Coulomb-distorted t matrix elements fulfill a set of LS equations

$$T^{cJ}_{\alpha\alpha_0}(k',k;E) = U^{cJ}_{\alpha\alpha_0}(k',k) + \sum_{\alpha'}\int_0^\infty dpp^2\ U^{cJ}_{\alpha\alpha'}(k,p)G_{C\alpha'}(E,p)T^{cJ}_{\alpha'\alpha_0}(p,k;E). \tag{B7}$$

Evaluating the Coulomb propagator $G_C(E)$ in the Coulomb basis leads to

$$G_{C\alpha}(E,p) = G_{0\alpha}(E,p) = (E - \varepsilon_\alpha - p^2/2\mu_\alpha + i\epsilon)^{-1}, \tag{B8}$$

where μ_α is the reduced mass in channel α. Here, $U^{cJ}_{\alpha\alpha_0}(k',k)$ are the potential matrix elements in the Coulomb basis. A direct evaluation of $U^{cJ}_{\alpha\alpha_0}(k',k)$ in momentum space is extremely difficult since the Coulomb wave functions are singular. Instead, it is evaluated using the nonsingular coordinate space Coulomb wave functions as described in Ref. [30].

Repeating the steps outlined in Sec. B 1, we obtain

$$t^{cJ}_{\alpha\beta}(k',k;E) = \sum_{\rho\sigma}\sum_{ij} T^{cJ}_{\alpha\rho}\left(k',k^\rho_i;E_i\right)\tau^{c,\,\rho\sigma}_{ij}(E)T^{cJ}_{\sigma\beta}\left(k,k^\sigma_j;E_j\right),$$
$$= \sum_{\rm ab} T^{cJ}_{\alpha a}(k',k_a;E_a)\tau^c_{\rm ab}(E)T^{cJ}_{b\beta}(k,k_b;E_b). \tag{B9}$$

The matrix $R^c_{\rm ab}(E)$ fulfills

$$\mathcal{M}^c_{\rm ab}(E) \equiv [R^c(E)\cdot\tau^c(E)]_{\rm ab}, \tag{B10}$$

where

$$R^c_{\rm ab}(E) = T^{cJ}_{\alpha_a\alpha_b}(k_b,k_a;E_a) + \sum_\beta\int_0^\infty dp\ p^2\ T^{cJ}_{\alpha_a,\beta}(p,k_a;E_a)G_{C\beta}(E_b)T^{cJ}_{\beta\alpha_b}(p,k_b;E_b)$$
$$- \sum_a \mathcal{M}^c_{\rm ad}(E)\sum_\beta\int_0^\infty dp\ p^2\ T^{cJ}_{\alpha_d\beta}(p,k_d;E_d)G_{C\beta}(E)T^{cJ}_{\beta\alpha_b}(p,k_b;E_b). \tag{B11}$$

The matrix $M^c_{\rm ad}(E)$ is given by

$$\mathcal{M}^c_{\rm ad}(E) \equiv [\mathcal{U}^{ce}(E)(\mathcal{U}^c)^{-1}]_{\rm ad}. \tag{B12}$$

APPENDIX C: DEFORMED OPTICAL MODEL POTENTIALS

Spherical optical model potentials (OMPs) are usually based on Woods-Saxon functions and depend on the distance between the nucleon and the surface of the nucleus, $r - R$. Nuclear deformations naturally lead to a deformed optical model potential (DOMP). The evaluation of the DOMP presented here follows closely that of Refs. [38,39]. For a

DOMP, the Woods-Saxon functions depend on the orientation of the nucleus so that $f_{\rm ws}(r,\theta,a,R) \equiv f_{\rm ws}(\tilde{r}(\theta),a,R)$, where the shifted radius is given as

$$\tilde{r}(\theta) = r - \delta(\hat{\xi}\cdot\hat{\mathbf{r}}). \tag{C1}$$

Here $\hat{\xi}$ represents the orientation of the nucleus relative to a space-fixed coordinate frame. The shift function $\delta(\xi\cdot\mathbf{r})$ is expanded in multipoles

$$\begin{aligned}\delta(\hat{\xi}\cdot\hat{\mathbf{r}}) &= \sum_{\lambda\neq 0}\delta_\lambda Y^0_\lambda(\theta,0),\\ &= \sum_{\lambda\neq 0,\,\mu}\frac{\sqrt{4\pi}}{\sqrt{2\lambda+1}}\delta_\lambda Y^{\mu *}_\lambda(\hat{\xi})Y^\mu_\lambda(\hat{\mathbf{r}}).\end{aligned} \tag{C2}$$

The angle θ is defined by $\cos\theta = \hat{\xi}\cdot\hat{\mathbf{r}}$. In the reference frame rotating with the nucleus, θ is simply the zenith angle of the relative vector $\mathbf{r}$. The deformation length δ_λ is proportional the maximum shift in the radius r at each multipole. Each term of the OMP is deformed independently and has the multipole expansion

$$\hat{U}(\xi,\mathbf{r}) = \sum_{\lambda\mu}\sqrt{4\pi}\hat{U}_\lambda(r)D^\lambda_{\mu,0}(\hat{\xi})Y^\mu_\lambda(\hat{\mathbf{r}}), \tag{C3}$$

where the rotational matrix is given by

$$D^\lambda_{\mu,0}(\hat{\xi}) = \frac{\sqrt{4\pi}}{\sqrt{2\lambda+1}}Y^{\mu *}_\lambda(\hat{\xi}). \tag{C4}$$

The expansion in Eq. (C3) can be written as

$$\begin{aligned}\hat{U}(\xi,\mathbf{r}) &= \sum_{\lambda\mu}\sqrt{4\pi}\hat{U}_\lambda(r)\frac{\sqrt{4\pi}}{\sqrt{2\lambda+1}}Y^{\mu *}_\lambda(\hat{\xi})Y^\mu_\lambda(\hat{\mathbf{r}})\\ &= \sum_\lambda\sqrt{4\pi}\hat{U}_\lambda(r)Y^0_\lambda(\theta,0),\end{aligned} \tag{C5}$$

$$= 4\pi\sum_\lambda(-1)^\lambda\hat{U}_\lambda(r)[Y_\lambda(\hat{\xi})\times Y_\lambda(\hat{\mathbf{r}})]^0_0. \tag{C6}$$

For each multipole λ, the potential is given by the angular integral

$$\begin{aligned}\hat{U}_\lambda(r) &= \sqrt{\pi}\int_{-1}^{1} d\cos\theta\; U(\tilde{r})Y^0_\lambda(\theta,0),\\ &= \frac{1}{2}\sqrt{2\lambda+1}\int_{-1}^{1} d\cos\theta\; U(\tilde{r})P_\lambda(\cos\theta).\end{aligned} \tag{C7}$$

This integral is zero for odd λ, which implies that $\hat{U}$ can only change the spin of the nucleus by an even number. For small deformations we can perform a Taylor expansion around $\tilde{r} = r$

$$U(\tilde{r}) = U(r) - U'(r)\sum_{\lambda\neq 0}\delta_\lambda Y^0_\lambda(\theta,0) + \cdots. \tag{C8}$$

The monopole term is given by

$$\hat{U}_0 = U(r), \tag{C9}$$

and for $\lambda > 0$ one obtains

$$\hat{U}_\lambda = -\frac{1}{\sqrt{4\pi}}\delta_\lambda U'(r). \tag{C10}$$

An alternative way of representing the deformation involves defining the deformation parameter

$$\beta_\lambda = \delta_\lambda/R. \tag{C11}$$

It is a measure of the deformation relative to the radius of the spherical potential. Such a deformation leads to the coupling of different angular momentum channels. To evaluate scattering observables using a deformed optical potential, one must solve a coupled set of Lippmann-Schwinger or Schrödinger equations.

A parametrization of a DOMP must specify, in addition to the the optical potential shape $U(r)$, the deformation length δ_λ or the deformation parameter β_λ. The multipole potential can then be evaluated according to Eq. (C7). For small deformation lengths, the multipole potentials are evaluated using Eqs. (C9) and (C10). In practice, only a few terms of the multipole expansion are necessary to describe elastic and inelastic nucleon-nucleus scattering. In order to constrain the DOMP, both elastic and inelastic scattering data are necessary.

1. The Olsson deformed optical model potential

Thus far we have described how a DOMP potential can be constructed starting from a spherical optical potential. We now focus on a a specific parametrization of the DOMP for the $n + {}^{12}$C system. The starting point is a spherical optical potential of the form

$$\begin{aligned}-U(r,E) = {}& V_r(E)\; f_{\rm ws}(r,a_r,R_r)\\ &+ 2V_{\rm so}(E)\left(\frac{-1}{r}\right)\frac{d}{dr}f_{\rm ws}(r,a_{\rm so},R_{\rm so})\,\mathbf{l}\cdot\boldsymbol{\sigma}\\ &+ iW_s(E)(-4a_s)\frac{d}{dr}f_{\rm ws}(r,a_s,R_s).\end{aligned} \tag{C12}$$

The real and imaginary strengths are indicated by $V(E)$ and $W(E)$. The indices r, so, i, and s denote the real volume, spin orbit, imaginary volume, and surface potential terms, respectively. The imaginary surface term is included to simulate the effects of a surface-peaked absorption at low energies, while at higher energies volume absorption dominates. The Woods-Saxon (WS) function is given by

$$f_{\rm ws}(r,a,R) = \left[1+\exp\left(\frac{r-R}{a}\right)\right]^{-1}, \tag{C13}$$

where a and R are the diffusiveness and radius. To proceed, deformations are introduced as described at the beginning of this section. This leads to a multichannel potential which is complex. The imaginary part simulates the effects of

TABLE I. Deformed optical potential parameters adjusted to $n + {}^{12}$C elastic and inelastic scattering data. These parameters are taken from Ref. [28]. Here, E_n is the neutron energy in the laboratory frame and should be given in MeV.

Strength (MeV)	Radius (fm)	Diffusiveness (fm)
$V_r = 64.02 - 0.674E_n$	$R_r = 1.093A^{1/3}$	$a_r = 0.619$
$W_s = 1.16 + 0.251E_n$	$R_s = 1.319A^{1/3}$	$a_s = 0.327$
$V_{\rm so} = 6.2$	$R_{\rm so} = 1.050A^{1/3}$	$a_{\rm so} = 0.550$

TABLE II. Parameters for the Meigooni [31] DOMP. Here, E is the proton energy in the laboratory frame and should be given in MeV.

Strength (MeV)	Radius (fm)	Diffusiveness (fm)
$V_r = 64.02 - 0.674E_n$	$R_r = 1.093A^{1/3}$	$a_r = 0.619$
$W_i(E) = 0$ for $E \leqslant 20$	$R_i = 1.22A^{1/3}$	$a_i = 0.478 + 0.0043E$
$W_i(E) = 15.5[1 - 2/(1 + \exp(E - 20)/25)]$ for $E > 20$		
$W_s(E) = e^{0.095E}$ for $E \leqslant 21$ MeV		
$W_s(E) = 10.29 - 0.145E$ for $21 \leqslant E < 71$ MeV	$R_s = 1.25A^{1/3}$	$a_s = 0.27$
$W_s(E) = 0$ for $E > 71$ MeV		
$V_{so} = 6.2$	$R_{so} = 1.050A^{1/3}$	$a_{so} = 0.550$

those processes that are not treated explicitly. The DOMP parameters include all the parameters of the spherical potential appearing in Eq. (C12) as well as the deformation parameters β_λ. In Ref. [28], Olsson and collaborators constrained these parameters of the DOMP by a simultaneous fit to cross sections for elastic and inelastic scattering of neutrons from ^{12}C for incident energies between 16 and 26 MeV. The multipole expansion is truncated at $\lambda = 4$ with the deformation parameters given as

$$\beta_2 = -0.65 \text{ and } \beta_4 = 0.05. \tag{C14}$$

For the reader's convenience, the remaining parameters are shown in Table I.

2. The Meigooni deformed optical model potential

The parametrization of the DOMP for proton-nucleus systems is carried in a similar manner as the neutron DOMP of Sec. C 1. The starting point is a spherical optical potential of the form

$$\begin{aligned} -U(r,E,A) = {} & V_r(E,A)\ f_{\rm ws}(r,a_r,R_r) \\ & + 2(V_{\rm so}(E,A))\left(\frac{-1}{r}\right)\frac{d}{dr} f_{\rm ws}(r,a_{\rm so},R_{\rm so})\,\mathbf{l}\cdot\boldsymbol{\sigma} \\ & + i\Big[W_i(E,A)\ f_{\rm ws}(r,a_i,R_i) + W_s(E,A)(-4a_s) \\ & \times \frac{d}{dr} f_{\rm ws}(r,a_s,R_s)\Big] + V_{\rm coul}(r,R_c), \end{aligned} \tag{C15}$$

where the $V_{\rm coul}(r,R_c)$ is the short-ranged Coulomb potential given by Eq. (38). As described in Sec. C 1, introducing deformations leads to a complex multichannel potential which must be treated within the coupled-channel formalism of Sec. II A 1. The parameters are adjusted to describe elastic and inelastic scattering data simultaneously. Meigooni and collaborators [31] fitted this form of the DOMP to differential cross sections for elastic and inelastic scattering of protons from ^{12}C. The deformation parameters have the values $\beta_2 = -0.61$ and $\beta_4 = 0.05$. The remaining parameters are shown in Table II for the reader's convenience.

[1] J. E. Escher, J. T. Burke, F. S. Dietrich, N. D. Scielzo, I. J. Thompson, and W. Younes, Rev. Mod. Phys. **84**, 353 (2012).
[2] R. L. Kozub, G. Arbanas, A. S. Adekola, D. W. Bardayan, J. C. Blockmon, K. Y. Chae, K. A. Chipps, J. A. Cizewski, R. Hatarik *et al.*, J. Phys. Conf. **420**, 012058 (2013).
[3] R. Kozub, G. Arbanas, A. Adekola, D. Bardayan, J. Blackmon *et al.*, Phys. Rev. Lett. **109**, 172501 (2012).
[4] F. M. Nunes and A. Deltuva, Phys. Rev. C **84**, 034607 (2011).
[5] K. Schmitt, K. Jones, A. Bey, S. Ahn, D. Bardayan *et al.*, Phys. Rev. Lett. **108**, 192701 (2012).
[6] A. Kankainen *et al.*, Eur. Phys. J. A **52**, 6 (2016).
[7] E. Alt, P. Grassberger, and W. Sandhas, Nucl. Phys. B **2**, 167 (1967).
[8] A. Deltuva and A. C. Fonseca, Phys. Rev. C **79**, 014606 (2009).
[9] A. Deltuva, A. C. Fonseca, and P. U. Sauer, Phys. Rev. C **71**, 054005 (2005).
[10] A. Deltuva, A. C. Fonseca, and P. U. Sauer, Phys. Rev. C **72**, 054004 (2005).
[11] F. M. Nunes and N. Upadhyay, J. Phys. G **403**, 012029 (2012).
[12] A. M. Mukhamedzhanov, V. Eremenko, and A. I. Sattarov, Phys. Rev. C **86**, 034001 (2012).
[13] A. Deltuva, Phys. Rev. C **88**, 011601 (2013).
[14] A. Deltuva, Nucl. Phys. A **947**, 173 (2016).
[15] E. A. Rauscher, J. O. Rasmussen, and K. Harada, Nucl. Phys. A **94**, 33 (1967).
[16] T. Tamura, Rev. Mod. Phys. **37**, 679 (1965).
[17] D. H. Feng, T. Udagawa, and T. Tamura, Nucl. Phys. A **274**, 262 (1976).
[18] L. Hlophe, C. Elster, R. C. Johnson, N. J. Upadhyay, F. M. Nunes, G. Arbanas, V. Eremenko, J. E. Escher, and J. J. Thompson (TORUS Collaboration), Phys. Rev. C **88**, 064608 (2013).
[19] L. Hlophe and C. Elster, Phys. Rev. C **93**, 034601 (2016).
[20] D. J. Ernst, C. M. Shakin, and R. M. Thaler, Phys. Rev. C **8**, 46 (1973).
[21] G. H. Rawitscher and G. Delic, Phys. Rev. C **29**, 1153 (1984).
[22] G. H. Rawitscher and G. Delic, Phys. Rev. C **29**, 747 (1984).
[23] K. Amos, L. Canton, P. R. Fraser, S. Karataglidis, J. P. Svenne, and D. van der Knijff, Eur. Phys. J. A **53**, 72 (2017).
[24] L. Canton, K. Amos, S. Karataglidis, G. Pisent, J. P. Svenne, and D. van der Knijff, Nucl. Phys. A **790**, 251 (2007).
[25] S. C. Pieper, Phys. Rev. C **9**, 883 (1974).
[26] W. Gloeckle, *The Quantum Mechanical Few-Body Problem*, Texts and Monographs in Physics (Springer Verlag, Berlin, 1983).

[27] I. J. Thompson and F. M. Nunes, *Nuclear Reactions for Astrophysics* (Cambridge University Press, Cambridge, UK, 2009).
[28] B. Olsson, B. Trostell, and E. Ramstrom, Nucl. Phys. A **496**, 505 (1989).
[29] L. Rodberg and R. Thaler, *Introduction of the Quantum Theory of Scattering*, Pure and Applied Physics Vol. 26 (Academic Press, San Deigo, CA, 1967).
[30] C. Elster, L. C. Liu, and R. M. Thaler, J. Phys. G **19**, 2123 (1993).
[31] A. S. Meigooni, R. W. Finlay, J. S. Petler, and J. P. Delaroche, Nucl. Phys. A **445**, 304 (1985).
[32] S. P. Weppner, R. B. Penney, G. W. Diffendale, and G. Vittorini, Phys. Rev. C **80**, 034608 (2009).
[33] E. Fabrici, S. Micheletti, M. Pignanelli, F. G. Resmini, R. De Leo, G. D'Erasmo, and A. Pantaleo, Phys. Rev. C **21**, 844 (1980).
[34] S. Kato, K. Okada, M. Kondo, K. Hosono, T. Saito, N. Matsuoka, K. Hatanaka, T. Noro, S. Nagamachi, H. Shimizu, K. Ogino, Y. Kadota, S. Matsuki, and M. Wakai, Phys. Rev. C **31**, 1616 (1985).
[35] A. Bohr and B. R. Mottelson, *Nuclear Strucure, Vol. II: Nuclear Deformations* (World Scientific, Weinheim, Germany, 1998).
[36] B. R. M. A. Bohr, Mat. Fys. **27**, 16 (1953).
[37] C. J. Joachain, *Quantum Collision Theory* (North Holland, 1976).
[38] D. M. Chase, L. Wilets, and A. R. Edmonds, Phys. Rev. **110**, 1080 (1958).
[39] B. Buck, Phys. Rev. **130**, 712 (1963).